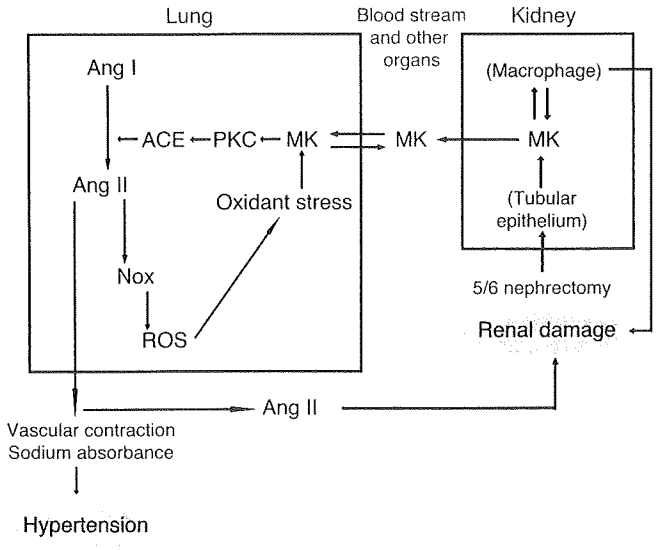

Figure 7
Schematic diagram showing the possible relationship between MK and the RAS cascade that promotes hypertension and renal damage.

MK protein and PTN protein. The recombinant human MK (rh-MK) was produced from yeast as described previously (48). In brief, human MK was produced by *Pichia pastoris* GS115 transfected with a human MK expression vector, which was constructed into pHIL-D4 (Invitrogen) (48). The MK protein was then purified by anion exchange chromatography and affinity chromatography on a heparin column. The purified human protein exhibited neurotrophic activity comparable to that of mouse MK produced in L cells (49). Recombinant human PTN was produced as previously described (50).

rh-MK and -PTN treatment model. In the pump study, MK protein in saline (1.6 mg/ml) (n = 5), PTN in saline (1.6 mg/ml; n = 5), or saline alone (n = 5) was infused using an osmotic pump (ALZA Corp.) into *Mdk*$^{-/-}$ mice after 5/6 nephrectomy. The pumps continuously infused a total of 100 μl over 14 days. The pumps were implanted under the dorsal skin the next day after 5/6 nephrectomy. Blood pressure was measured by the indirect tail-cuff technique at 0 and 2 weeks after 5/6 nephrectomy. Mice were sacrificed at 2 weeks after 5/6 nephrectomy, and blood and tissue samples were collected.

Blood pressure monitoring. Blood pressure was measured in restrained, conscious mice by the indirect tail-cuff technique under unstressed conditions (BP-98A; Softron) at 0, 2, 4, 6, and 8 weeks after 5/6 nephrectomy (51). Before measurement, the mice were warmed with a heating pad for 5 minutes. A total of 7–10 readings were taken for each mouse, at 1- to 2-minute intervals.

Sample collection. Mice were sacrificed at 2, 4, and 8 weeks after 5/6 nephrectomy. The remnant kidney, lung, brain, heart, and liver were removed rapidly, snap-frozen in liquid nitrogen, and stored at -80°C until examinations were performed. Each tissue was processed for histology, protein extraction, and RNA extraction. Blood samples were collected into chilled tubes for measurement of renal function parameters and into chilled tubes containing EDTA for Ang II measurements. Serum and plasma were separated by centrifugation (500 *g* for 10 minutes) and stored at -80°C until measurement were performed. Serum creatinine, blood urea nitrogen (*Mdk*$^{+/+}$: sham, n = 6; 2 weeks, n = 10; 4 weeks, n = 9; 8 weeks, n = 8; *Mdk*$^{-/-}$: sham, n = 7; 2 weeks, n = 7; 4 weeks, n = 6; 8 weeks, n = 4), and Ang II concentrations (*Mdk*$^{+/+}$: sham, n = 6; 2 weeks, n = 6; 4 weeks, n = 8; *Mdk*$^{-/-}$: sham, n = 6; 2 weeks, n = 7; 4 weeks, n = 5) were measured by Mitsubishi BCL.

ACE activity assay. Lung ACE activity was measured in a fluorescence assay using a commercial ACE activity assay kit (Life Laboratory Company, Yamagata, Japan). Isolated lung tissue (*Mdk*$^{+/+}$: sham, n = 5; 2 weeks, n = 5; 4 weeks, n = 5; *Mdk*$^{-/-}$: sham, n = 5; 2 weeks, n = 5; 4 weeks, n = 4) was homogenized in an assay buffer and then clarified by centrifugation at 10,000 *g* for 15 minutes at 4.0°C. ACE activity against a synthetic substrate (benzyloxycarbonyl-phenyl alanyl-leucine) was determined using a colorimetric method. The product was measured fluorometrically at 355-nm excitation and 460-nm emission with a fluoro-colorimeter, as follows. For the assay, tissue samples were standardized to 1 μg protein/ml. Results were calculated as mU/mg protein. All data are reported as mean ± SD. The measurements were performed in duplicate.

Histology and immunohistochemistry. The removed kidneys and lungs were fixed in 10% buffered formalin, embedded in paraffin, and then cut into 4-μm sections. The sections were stained with H&E, PAS, and Masson's trichrome. Another tissue sample was embedded in OCT compound (Sakura Finetek) and frozen in liquid nitrogen for immunostaining. Sections were cut to a thickness of 3 μm with a cryostat and fixed in acetone. High-power fields were used to examine the sections for evidence of focal sclerosis (52, 53). Glomerular sclerosis was assessed by semiquantitative score (grades 0 to +4) using the method of Raij et al. (54): grade 0, no sclerosis of glomeruli; grade 1, sclerosis of up to 25% of glomerulus; grade 2, sclerosis of 25%–50% of glomerulus; grade 3, sclerosis of 50%–75% of glomerulus; grade 4, sclerosis of 75%–100% of glomerulus. At least 50 glomeruli were evaluated under ×400 magnification and results averaged for each kidney (*Mdk*$^{+/+}$: 2 weeks, n = 5; 4 weeks, n = 4; 8 weeks, n = 4; *Mdk*$^{-/-}$: 2 weeks, n = 4; 4 weeks, n = 3; 8 weeks, n = 3). Immunostaining for ACE and MK was performed on buffered formalin-fixed tissues. Sections were deparaffinized, rehydrated, incubated in 3% hydrogen peroxide in methanol to block endogenous peroxidase, and washed in 10% normal goat serum (Dako) in PBS to block nonspecific binding. Subsequently, sections were incubated with mouse anti-ACE monoclonal antibody (dilution, 1:400; Chemicon International, Millipore) or anti-MK monoclonal antibody (dilution, 1:100) overnight at 4°C as described previously (22), followed by a conjugate of polyclonal goat anti-mouse IgG antibody and HRP-labeled polymer (Histofine Simple Stain; Nichirei) for 1 hour at room temperature as a secondary antibody. The staining was visualized with 3-3′ diaminobenzidine (Nichirei) to produce a brown color. The sections were covered with 90% glycerol containing *p*-phenylenediamine and were examined by electron microscopy (H-7100; Hitachi). For double immunofluorescence staining of MK and thrombomodulin as a marker of the vascular endothelium, the cryosections of lungs were first incubated with chicken anti-human MK (dilution, 1:200) and then with rabbit anti-rat thrombomodulin (dilution, 1:1,000) (55), followed by incubation with FITC-labeled rabbit anti-chicken IgG (dilution, 1:160) and rhodamine-labeled goat anti-rabbit IgG (dilution, 1:320) as secondary antibodies. For immunofluorescence staining of macrophages and neutrophils, the cryosections of lungs or kidneys were first incubated with rat anti-mouse F4/80 antibodies (MCA497F; dilution, 1:50; AbD Serotec) or rat anti-mouse neutrophils (MCA771G; dilution, 1:200; AbD Serotec), followed by incubation with FITC-labeled goat anti-rat IgG F(ab)′ 2 (dilution, 1:160) or FITC-labeled rabbit anti-rat IgG (dilution, 1:160) as secondary antibodies. The lung and kidney section from each mouse was viewed under ×400 magnification, and then macrophages or neutrophils were counted from 10 fields and averaged. Values are mean ± SD.

HMVEC-L culture and treatments. HMVEC-L were used for the in vitro assay because they have previously been shown to express ACE (56). HMVEC-L (Takara Bio Inc.) were cultivated in EGM-2MV BulletKit medium (Takara Bio Inc.) at 37°C in 5% CO_2. HMVEC-L were grown as a monolayer in tissue culture plates coated with type I collagen. When the cells reached 70%–80% confluence, they were passaged with trypsin (0.025%)/EDTA (0.01%) and used within 4 passages, as recommended by the supplier. After reaching

confluence, HMVEC-L were washed with PBS and cultured for 24 hours in essential basal medium containing 0.5% FBS. These cells were exposed to 100 ng/ml recombinant human MK (rh-MK) plus 20 μg/ml heparin or 50 ng/ml PMA (Sigma-Aldrich) in essential basal medium containing 0.5% FBS. PMA and the PKC inhibitor stock solutions were made in dimethyl sulfoxide. For PKC inhibition, BIS (Calbiochem) was added 1 hour before treatment with rh-MK plus heparin or PMA. Protein was extracted from HMVEC-L at the indicated time points after treatment. Cells were then lysed in RIPA buffer (50 mmol/l Tris-HCl, 150 mmol/l NaCl, 1% Nonidet P-40, 1% deoxycholic acid, and 0.05% sodium dodecyl sulfate) containing 0.25 mmol/l phenylmethylsulfonyl fluoride, kept on ice for 40 minutes, and then centrifuged at 15,000 *g* for 10 minutes at 4°C. The supernatants were then subjected to SDS-PAGE and Western blotting.

Ang II concentration in HMVEC-L. After reaching confluence, HMVEC-L were washed with PBS and cultured for 24 hours in essential basal medium containing 0.5% FBS. These cells were exposed to 100 ng/ml rh-MK plus 20 μg/ml heparin or 20 μg/ml heparin alone in essential basal medium containing 0.5% FBS for 36 hours. After stimulation, HMVEC-L were washed with PBS and exposed to 500 pM Ang I (Sigma-Aldrich) for 10 and 25 minutes. Supernatants were collected into chilled tubes, and then the Ang II concentration was measured as previously described (57).

Western blot analysis. Mouse kidney, lung, brain, heart, and liver tissues were snap-frozen in liquid nitrogen for protein isolation. Western blot analysis was performed as described previously (58). The blots were subsequently incubated with goat anti-human MK antibody (dilution, 1:1,000), monoclonal anti-β-actin antibody (dilution, 1:1,000; Sigma-Aldrich), mouse anti-ACE monoclonal antibody (dilution, 1:1,000; Chemicon International, Millipore), or rabbit anti-phospho-PKC antibody (dilution, 1:1,000; Cell Signaling Technology), followed by incubation with peroxidase-conjugated goat IgG, mouse IgG, or rabbit IgG (dilution, 1:5,000; Jackson Immunoresearch Laboratories Inc.). Western blot analysis of liver ANG was performed using the ANG-specific polyclonal antibody as described previously (59). Proteins were visualized with an enhanced chemiluminescence detection system (Amersham Pharmacia, GE Healthcare). The density of each band was measured using the public domain NIH Image program (http://rsb.info.nih.gov/nih-image/).

RNA preparation from mouse kidney and lung. Mouse kidney and lung tissues (15 mg) were immersed in RNA*later* (Ambion, Applied Biosystems) for 1 day. The mixture was ground for 2 minutes with 5-mm tungsten carbide beads at a frequency of 20–25 Hz using a mixer-mill grinder according to the manufacturer's instructions (Tissuelyser; QIAGEN). The ground solution was then centrifuged for 3 minutes at 10,000 *g* to compact the debris, and the supernatant was treated according to the manufacturer's instructions. Total RNA was extracted using an RNeasy Mini Kit (QIAGEN). RNA concentrations were estimated using a spectrophotometer (Ultrospec 3300 pro; Amersham Biosciences, GE Healthcare).

Real-time PCR. First-strand cDNA was synthesized using the Quanti-Tect Reverse Transcription Kit (QIAGEN) according to the manufacturer's instructions. One microgram of total RNA was then reverse transcribed. To validate changes in gene expression, we performed real-time PCR analysis with an Applied Biosystems Prism 7500HT Sequence Detection System using TaqMan Gene Expression Assays according to the manufacturer's specifications (Applied Biosystems). Two microliters of cDNA samples was used for the PCR reaction. The TaqMan probes and primers were as follows. For mouse MK: forward, 5′-CAAGGGACCCT-GAAGAAGGC-3′, and reverse, 5′-CTTTGGTCTTTGACTTGCTCTTGG-3′; for ANG: forward, 5′-CTCGAACTCAAAGCAGGAGAGG-3′, and reverse, 5′-CGTAGATGGCGAACAGGAAGG-3′; for renin: 5′-TTGTTGCTCTG-GAGTCCTTGC-3′, and reverse, 5′-CAGGATTTCCCGGACAGAAGG-3′; for ACE: forward, 5′-ACCCAACCTCGATGTCACCA-3′, and reverse, 5′-GCGAGGTGAAGAATTCCTCTGA-3′; for Nox1: forward, 5′-TTG-GCACAGTCAGTGAGGATG-3′, and reverse, 5′-AGATTTCAAGATG-GAAGCAAAGGG-3′; for Nox2: forward, 5′-ACTTTCCATAAGATG-GTAGCTTGG-3′, and reverse, 5′-GCATTCACACACCACTCAACG-3′; and for Nox4: forward, 5′-ACCAGAATGAGGATCCCAGAAAG-3′, and reverse, 5′-GTAGAAGCTGTAACCATGAGGAAC-3′. 18S ribosomal RNA (assay identification number 4326317E), which was used as an endogenous control, was as assay-on-demand gene expression product (Applied Biosystems). The thermal cycler conditions were as follows: hold for 10 minutes at 95°C, followed by 2-step PCR consisting of 40 cycles at 95°C for 15 seconds and 60°C for 1 minute. The relative quantification of all targets was carried out using the comparative cycle threshold method (60). The levels of gene expression were standardized with those of the 18S ribosomal RNA.

Statistics. Results are expressed as mean ± SD. Statistical difference was assessed by a single-factor variance (ANOVA) followed by a 2-tailed unpaired *t* test, as appropriate. *P* values less than 0.05 were considered significant.

Acknowledgments

We thank Norihiko Suzuki, Naoko Asano, Yuriko Sawa, and Kayoko Miyata for their excellent technical assistance. This work was supported in part by the 21st Century COE Program and Global COE program, Ministry of Education, Culture, Sports, Science, and Technology, Japan.

Received for publication August 25, 2008, and accepted in revised form March 25, 2009.

Address correspondence to: Kenji Kadomatsu, Department of Biochemistry, Nagoya University Graduate School of Medicine, 65 Tsurumai-cho, Showa-ku, Nagoya 466-8550, Japan. Phone: 81-52-744-2059; Fax: 81-52-744-2065; E-mail: kkadoma@med.nagoya-u.ac.jp.

1. Atlas, S.A. 2007. The renin-angiotensin aldosterone system: pathophysiological role and pharmacologic inhibition. *J. Manag. Care Pharm.* **13**:9–20.
2. Kobori, H., Nangaku, M., Navar, L.G., and Nishiyama, A. 2007. The intrarenal renin-angiotensin system: from physiology to the pathobiology of hypertension and kidney disease. *Pharmacol. Rev.* **59**:251–287.
3. Ruster, C., and Wolf, G. 2006. Renin-angiotensin-aldosterone system and progression of renal disease. *J. Am. Soc. Nephrol.* **17**:2985–2991.
4. Skeggs, L.T., Jr., Kahn, J.R., Lentz, K., and Shumway, N.P. 1957. The preparation, purification, and amino acid sequence of a polypeptide renin substrate. *J. Exp. Med.* **106**:439–453.
5. Dzau, V.J. 1988. Tissue renin-angiotensin system: physiologic and pharmacologic implications. Introduction. *Circulation.* **77**:I1–I3.
6. Sayed-Tabatabaei, F.A., Oostra, B.A., Isaacs, A., van Duijn, C.M., and Witteman, J.C. 2006. ACE polymorphisms. *Circ. Res.* **98**:1123–1133.
7. Remuzzi, G., Perico, N., Macia, M., and Ruggenenti, P. 2005. The role of renin-angiotensin-aldosterone system in the progression of chronic kidney disease. *Kidney Int. Suppl.* S57–S65.
8. Kadomatsu, K., and Muramatsu, T. 2004. Midkine and pleiotrophin in neural development and cancer. *Cancer Lett.* **204**:127–143.
9. Sato, W., et al. 2005. Midkine antisense oligodeoxyribonucleotide inhibits renal damage induced by ischemic reperfusion. *Kidney Int.* **67**:1330–1339.
10. Kosugi, T., et al. 2006. Growth factor midkine is involved in the pathogenesis of diabetic nephropathy. *Am. J. Pathol.* **168**:9–19.
11. Ezquerra, L., Herradon, G., Nguyen, T., Silos-Santiago, I., and Deuel, T.F. 2005. Midkine, a newly discovered regulator of the renin-angiotensin pathway in mouse aorta: significance of the pleiotrophin/midkine developmental gene family in angiotensin II signaling. *Biochem. Biophys. Res. Commun.* **333**:636–643.
12. Werner, C., et al. 2008. RAS blockade with ARB and ACE inhibitors: current perspective on rationale and patient selection. *Clin. Res. Cardiol.* **97**:418–431.
13. Wuhl, E., and Schaefer, F. 2008. Therapeutic strategies to slow chronic kidney disease progression. *Pediatr. Nephrol.* **23**:705–716.
14. Ferrari, P. 2007. Prescribing angiotensin-converting enzyme inhibitors and angiotensin receptor blockers in chronic kidney disease. *Nephrology (Carlton).* **12**:81–89.

15. Olson, J.L., Hostetter, T.H., Rennke, H.G., Brenner, B.M., and Venkatachalam, M.A. 1982. Altered glomerular permselectivity and progressive sclerosis following extreme ablation of renal mass. *Kidney Int.* **22**:112–126.
16. Hostetter, T.H., Olson, J.L., Rennke, H.G., Venkatachalam, M.A., and Brenner, B.M. 1981. Hyperfiltration in remnant nephrons: a potentially adverse response to renal ablation. *Am. J. Physiol.* **241**:F85–F93.
17. Dikow, R., et al. 2004. Increased infarct size in uremic rats: reduced ischemia tolerance? *J. Am. Soc. Nephrol.* **15**:1530–1536.
18. van Dokkum, R.P., et al. 2004. Myocardial infarction enhances progressive renal damage in an experimental model for cardio-renal interaction. *J. Am. Soc. Nephrol.* **15**:3103–3110.
19. Pupilli, C., Chevalier, R.L., Carey, R.M., and Gomez, R.A. 1992. Distribution and content of renin and renin mRNA in remnant kidney of adult rat. *Am. J. Physiol.* **263**:F731–F738.
20. Nishimura, M., Takahashi, H., and Yoshimura, M. 2007. Upregulation of the brain renin-angiotensin system in rats with chronic renal failure. *Acta Physiol. (Oxf.).* **189**:369–377.
21. Riordan, J.F. 2003. Angiotensin-I-converting enzyme and its relatives. *Genome Biol.* **4**:225.
22. Sato, W., et al. 2001. Midkine is involved in neutrophil infiltration into the tubulointerstitium in ischemic renal injury. *J. Immunol.* **167**:3463–3469.
23. Narita, H., Chen, S., Komori, K., and Kadomatsu, K. 2008. Midkine is expressed by infiltrating macrophages in in-stent restenosis in hypercholesterolemic rabbits. *J. Vasc. Surg.* **47**:1322–1329.
24. Inoh, K., Muramatsu, H., Ochiai, K., Torii, S., and Muramatsu, T. 2004. Midkine, a heparin-binding cytokine, plays key roles in intraperitoneal adhesions. *Biochem. Biophys. Res. Commun.* **317**:108–113.
25. Villard, E., Alonso, A., Agrapart, M., Challah, M., and Soubrier, F. 1998. Induction of angiotensin I-converting enzyme transcription by a protein kinase C-dependent mechanism in human endothelial cells. *J. Biol. Chem.* **273**:25191–25197.
26. Touyz, R.M. 2003. Reactive oxygen species in vascular biology: role in arterial hypertension. *Expert Rev. Cardiovasc. Ther.* **1**:91–106.
27. Vaziri, N.D., and Rodriguez-Iturbe, B. 2006. Mechanisms of disease: oxidative stress and inflammation in the pathogenesis of hypertension. *Nat. Clin. Pract. Nephrol.* **2**:582–593.
28. Hoke, T.S., et al. 2007. Acute renal failure after bilateral nephrectomy is associated with cytokine-mediated pulmonary injury. *J. Am. Soc. Nephrol.* **18**:155–164.
29. Kelly, K.J. 2003. Distant effects of experimental renal ischemia/reperfusion injury. *J. Am. Soc. Nephrol.* **14**:1549–1558.
30. Anavekar, N.S., et al. 2004. Relation between renal dysfunction and cardiovascular outcomes after myocardial infarction. *N. Engl. J. Med.* **351**:1285–1295.
31. Amann, K., Wanner, C., and Ritz, E. 2006. Cross-talk between the kidney and the cardiovascular system. *J. Am. Soc. Nephrol.* **17**:2112–2119.
32. Kuczera, M., et al. 1991. Local angiotensin formation in hindlimbs of uremic hypertensive and renovascular hypertensive rats. *J. Hypertens.* **9**:41–48.
33. Kidney Disease Outcomes Quality Initiative (K/DOQI). 2004. K/DOQI clinical practice guidelines on hypertension and antihypertensive agents in chronic kidney disease. *Am. J. Kidney Dis.* **43**(5 Suppl. 1):S1–S290.
34. Iannone, A., Bini, A., Swartz, H.M., Tomasi, A., and Vannini, V. 1989. Metabolism in rat liver microsomes of the nitroxide spin probe tempol. *Biochem. Pharmacol.* **38**:2581–2586.
35. Schnackenberg, C.G., and Wilcox, C.S. 1999. Two-week administration of tempol attenuates both hypertension and renal excretion of 8-Iso prostaglandin f2alpha. *Hypertension.* **33**:424–428.
36. Johnson, F., and Giulivi, C. 2005. Superoxide dismutases and their impact upon human health. *Mol. Aspects Med.* **26**:340–352.
37. Mollnau, H., et al. 2002. Effects of angiotensin II infusion on the expression and function of NAD(P)H oxidase and components of nitric oxide/cGMP signaling. *Circ. Res.* **90**:E58–E65.
38. Liao, T.D., et al. 2008. Role of inflammation in the development of renal damage and dysfunction in angiotensin II-induced hypertension. *Hypertension.* **52**:256–263.
39. Kobori, H., Prieto-Carrasquero, M.C., Ozawa, Y., and Navar, L.G. 2004. AT1 receptor mediated augmentation of intrarenal angiotensinogen in angiotensin II-dependent hypertension. *Hypertension.* **43**:1126–1132.
40. Graciano, M.L., et al. 2008. Purinergic receptors contribute to early mesangial cell transformation and renal vessel hypertrophy during angiotensin II-induced hypertension. *Am. J. Physiol. Renal Physiol.* **294**:F161–F169.
41. Horiba, M., et al. 2000. Neointima formation in a restenosis model is suppressed in midkine-deficient mice. *J. Clin. Invest.* **105**:489–495.
42. Tu, X., et al. 2008. Anti-inflammatory renoprotective effect of clopidogrel and irbesartan in chronic renal injury. *J. Am. Soc. Nephrol.* **19**:77–83.
43. Usui, H.K., et al. 2007. Macrophage scavenger receptor-a-deficient mice are resistant against diabetic nephropathy through amelioration of microinflammation. *Diabetes* **56**:363–372.
44. Nakamura, E., et al. 1998. Disruption of the midkine gene (Mdk) resulted in altered expression of a calcium binding protein in the hippocampus of infant mice and their abnormal behaviour. *Genes Cells.* **3**:811–822.
45. Sada, T., Koike, H., Nishino, H., and Oizumi, K. 1989. Chronic inhibition of angiotensin converting enzyme decreases Ca2+-dependent tone of aorta in hypertensive rats. *Hypertension.* **13**:582–588.
46. Yoshida, K., Xu, H.L., Kawamura, T., Ji, L., and Kohzuki, M. 2002. Chronic angiotensin-converting enzyme inhibition and angiotensin II antagonism in rats with chronic renal failure. *J. Cardiovasc. Pharmacol.* **40**:533–542.
47. Nishiyama, A., et al. 2004. Possible contributions of reactive oxygen species and mitogen-activated protein kinase to renal injury in aldosterone/salt-induced hypertensive rats. *Hypertension.* **43**:841–848.
48. Ikematsu, S., et al. 2000. Serum midkine levels are increased in patients with various types of carcinomas. *Br. J. Cancer.* **83**:701–706.
49. Muramatsu, H., and Muramatsu, T. 1991. Purification of recombinant midkine and examination of its biological activities: functional comparison of new heparin binding factors. *Biochem. Biophys. Res. Commun.* **177**:652–658.
50. Murasugi, A., Kido, I., Kumai, H., and Asami, Y. 2003. Efficient production of recombinant human pleiotrophin in yeast, Pichia pastoris. *Biosci. Biotechnol. Biochem.* **67**:2288–2290.
51. Pfeffer, J.M., Pfeffer, M.A., and Frohlich, E.D. 1971. Validity of an indirect tail-cuff method for determining systolic arterial pressure in unanesthetized normotensive and spontaneously hypertensive rats. *J. Lab. Clin. Med.* **78**:957–962.
52. Kohzuki, M., et al. 1995. Kinin and angiotensin II receptor antagonists in rats with chronic renal failure: chronic effects on cardio- and renoprotection of angiotensin converting enzyme inhibitors. *J. Hypertens.* **13**:1785–1790.
53. Saito, T., et al. 1990. Progression of experimental focal glomerulosclerosis in the spontaneously hypertensive rat. *J. Lab. Clin. Med.* **115**:165–173.
54. Raij, L., Azar, S., and Keane, W. 1984. Mesangial immune injury, hypertension, and progressive glomerular damage in Dahl rats. *Kidney Int.* **26**:137–143.
55. Yuzawa, Y., et al. 1993. Antibody-mediated redistribution and shedding of endothelial antigens in the rabbit. *J. Immunol.* **150**:5633–5646.
56. Shen, J., Ham, R.G., and Karmiol, S. 1995. Expression of adhesion molecules in cultured human pulmonary microvascular endothelial cells. *Microvasc. Res.* **50**:360–372.
57. Nishiyama, A., Seth, D.M., and Navar, L.G. 2002. Renal interstitial fluid concentrations of angiotensins I and II in anesthetized rats. *Hypertension.* **39**:129–134.
58. Kadomatsu, K., et al. 1997. Midkine induces the transformation of NIH3T3 cells. *Br. J. Cancer.* **75**:354–359.
59. Kobori, H., Harrison-Bernard, L.M., and Navar, L.G. 2001. Expression of angiotensinogen mRNA and protein in angiotensin II-dependent hypertension. *J. Am. Soc. Nephrol.* **12**:431–439.
60. Livak, K.J., and Schmittgen, T.D. 2001. Analysis of relative gene expression data using real-time quantitative PCR and the 2(-delta delta C(T)) method. *Methods.* **25**:402–408.

BASIC RESEARCH www.jasn.org

The E-Selectin Ligand Basigin/CD147 Is Responsible for Neutrophil Recruitment in Renal Ischemia/Reperfusion

Noritoshi Kato,*† Yukio Yuzawa,† Tomoki Kosugi,*† Akinori Hobo,*† Waichi Sato,† Yuko Miwa,* Kazuma Sakamoto,* Seiichi Matsuo,† and Kenji Kadomatsu*

Departments of *Biochemistry and †Nephrology, Nagoya University Graduate School of Medicine, Nagoya, Japan

ABSTRACT

E-selectin and its ligands are essential for extravasation of leukocytes in inflammation. Here, we report that basigin (Bsg)/CD147 is a ligand for E-selectin that promotes renal inflammation in ischemia/reperfusion. Compared with wild-type mice, Bsg-deficient ($Bsg^{-/-}$) mice demonstrated striking suppression of neutrophil infiltration in the kidney after renal ischemia/reperfusion. Although E-selectin expression increased similarly between the two genotypes, $Bsg^{-/-}$ mice exhibited less renal damage, suggesting that Bsg on neutrophils contribute to renal injury in this model. Neutrophils expressed Bsg with *N*-linked polylactosamine chains and $Bsg^{-/-}$ neutrophils showed reduced binding to E-selectin. Bsg isolated from HL-60 cells bound to E-selectin, and tunicamycin treatment to abolish *N*-linked glycans from Bsg abrogated this binding. Furthermore, $Bsg^{-/-}$ neutrophils exhibited reduced E-selectin-dependent adherence to human umbilical vein endothelial cells *in vitro*. Injection of labeled neutrophils into mice showed that $Bsg^{-/-}$ neutrophils were less readily recruited to the kidney after renal ischemia/reperfusion than $Bsg^{+/+}$ neutrophils, regardless of the recipient's genotype. Taken together, these results indicate that Bsg is a physiologic ligand for E-selectin that plays a critical role in the renal damage induced by ischemia/reperfusion.

J Am Soc Nephrol 20: 1565–1576, 2009. doi: 10.1681/ASN.2008090957

The selectins and their ligands are essential for leukocyte tethering/rolling on endothelial cells and the initiation of inflammatory response. The selectins are C-type lectins and consist of three members, *i.e.*, P-, L-, and E-selectin.[1,2] P-selectin is expressed upon inflammatory stimulation in platelets and endothelial cells. L-selectin is constitutively expressed on the tip of leukocyte microvilli and implicated in lymphocyte homing to lymph nodes.[3] E-selectin is specifically induced in the endothelium upon inflammatory stimulation. Thus, E- and P-selectin closely collaborate with one another and play a major role in leukocyte recruitment to inflammatory sites.[4–6] Among the several glycoproteins reported to bind to E-selectin, three have been identified as representative physiologic E-selectin ligands on neutrophils. There are P-selectin glycoprotein ligand-1 (PSGL-1), E-selectin ligand-1, and CD44, and all three play distinct roles during tethering and slow rolling of neutrophils on the endothelium.[7] A minimal recognition motif for all selectins is sialylated and fucosylated glycan determinants, such as sialyl Lewis X, that decorate the terminal extensions of carbohydrates of these molecules.[8,9] However, because of the poor immunogenicity of highly gly-

Received September 12, 2008. Accepted February 27, 2009.

Published online ahead of print. Publication date available at www.jasn.org.

Correspondence: Kenji Kadomatsu, Department of Biochemistry, Nagoya University Graduate School of Medicine, 65 Tsurumacho, Showa-ku, Nagoya 466-8550, Japan. Phone: +81-52-744-2060; Fax: +81-52-744-2065; E-mail: kkadoma@med.nagoya-u.ac.jp

Copyright © 2009 by the American Society of Nephrology

cosylated epitopes, it has proven difficult to identify selectin ligands.

Basigin (Bsg)/CD147 (*Bsg* is the name of the mouse gene) is a membrane glycoprotein that belongs to the Ig superfamily. Bsg was discovered in embryonal carcinoma cells as a receptor for *Lotus tetragonolobus* agglutinin[10] and was determined to have the structure Galβ1→4(Fucα1→3)GlcNAc, which is known as the Lewis X structure. But it has been unclear whether Bsg has sialyl Lewis X structure and whether Bsg serves as a selectin ligand. Bsg is expressed in many cell types, *e.g.*, blood cells, epithelial cells, endothelial cells, and germ cells. We previously generated *Bsg*-deficient ($Bsg^{-/-}$) mice and found several abnormalities that included male and female sterility, progressive retinal degeneration, increased cell proliferation upon mixed lymphocyte culture, decreased memory function, and abnormal sensory function.[11–13] In addition to these functions deduced through the study of $Bsg^{-/-}$ mice, two additional Bsg functions have recently been highlighted. First, Bsg activates matrix metaloproteases (MMPs), thereby promoting cancer invasion.[14] Second, Bsg functions like a chaperone for monocarboxylate transporters (MCTs).[15,16] In the present study, we found an additional and unexpected role of Bsg; namely, its glycosylation was crucial for inflammation.

Acute kidney injury (AKI) is a common complication that occurs in approximately 5% of hospitalized patients and in approximately 30% of patients in intensive care units. As the mortality of AKI is still unacceptably high, between 40% and 60%,[17] this disease is being intensively studied. Renal ischemia/reperfusion injury is characteristic of acute renal inflammation involving marked infiltration of inflammatory cells, such as neutrophils, and is the most widely used model for human AKI.[18] We used this model to investigate the role of Bsg in inflammation in the present study. $Bsg^{-/-}$ mice exhibited less renal damage after ischemia/reperfusion. To our surprise, this phenotype was attributable to Bsg on neutrophils, rather than Bsg on other cells in the inflammation area. We found that highly glycosylated Bsg on neutrophils bound to E-selectin on endothelial cells and led to neutrophil infiltration to the inflammatory lesion. Our results may shed light on the mechanisms underlying the pathogenesis of AKI.

RESULTS

Bsg Deficiency Preserves Renal Function and Decreases Renal Injury after Ischemia/Reperfusion

We subjected $Bsg^{+/+}$ and $Bsg^{-/-}$ mice to renal ischemia/reperfusion injury. As shown in Figure 1, the renal damage was less pronounced in $Bsg^{-/-}$ mice than in $Bsg^{+/+}$ mice. Thus, 2 d after ischemia/reperfusion, $Bsg^{-/-}$ mice showed less tubulointerstitial injury by all three criteria examined, *i.e.*, tubular cast formation, dilation, and degeneration (Figure 1, A and B). The increase of serum urea nitrogen levels was also significantly suppressed in $Bsg^{-/-}$ mice (Figure 1C). The serum urea nitrogen reached the maximum level on day 1 after ischemia in $Bsg^{-/-}$ mice versus day 2 in $Bsg^{+/+}$ mice. Thus, postischemic renal injury was quickly terminated in $Bsg^{-/-}$ mice.

Bsg Deficiency Reduces Neutrophil Infiltration into the Tubulointerstitium

Renal ischemia/reperfusion injury is characterized by a massive influx of neutrophils early after reperfusion, which plays a crucial role in the pathogenesis of postischemic renal failure through the release of cytotoxic proteases and oxygen-derived

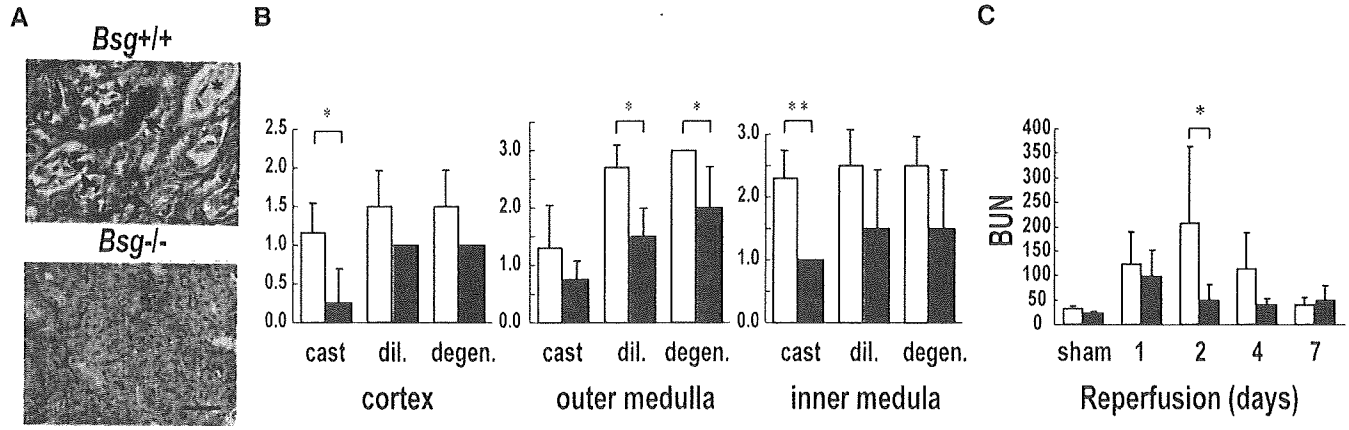

Figure 1. Renal injury is less severe in $Bsg^{-/-}$ mice after renal ischemia/reperfusion. (A) A representative image of tubular lesions 2 d after ischemia/reperfusion injury. Less renal damage was observed in $Bsg^{-/-}$ mice than in $Bsg^{+/+}$ mice. Arrow, tubular cast; arrowhead, degeneration of the tubule; asterisk, dilation of the tubule. Scale bar, 50 μm. Periodic acid-Schiff staining. (B) Semiquantitative analysis of tubulointerstitial damage 2 d after ischemia/reperfusion injury. The degree of tubular cast formation, tubular dilation, and tubular degeneration were comparatively rated as described in the Concise Methods section. High values indicate more severe damage. White columns, $Bsg^{+/+}$ mice; black columns, $Bsg^{-/-}$ mice. cast, cast formation. dil., dilation. degen., degeneration. Data are means (columns) and SEM; bars). $^*P < 0.05$; $^{**}P < 0.01$; $n = 6$. (C) Blood urea nitrogen (BUN) levels in $Bsg^{+/+}$ and $Bsg^{-/-}$ mice after ischemia/reperfusion. Renal function was better preserved in $Bsg^{-/-}$ than $Bsg^{+/+}$ mice. White columns, $Bsg^{+/+}$ mice; black columns, $Bsg^{-/-}$ mice. BUN is shown as mg/dl. Data are means (columns) and SEM (bars). $^*P < 0.05$; $n = 6$.

radicals.[19] We next compared the amount of neutrophil influx and renal function. Bsg deficiency greatly reduced the influx of neutrophils to the kidney 1 d after ischemia/reperfusion (Figure 2A). The number of infiltrated neutrophils reached the maximum level 1 d after ischemia/reperfusion (Figure 2A). This was in contrast to the macrophage influx, which peaked 4 d after ischemia/reperfusion (Figure 2B). As the difference in renal function between $Bsg^{+/+}$ and $Bsg^{-/-}$ mice became apparent 2 d after ischemia/reperfusion (Figure 1C), it is conceivable that neutrophil influx, rather than macrophage influx, was crucial for the role of Bsg in renal damage in our model.

It is widely accepted that chemokines are generated by ischemic tubular epithelial cells in the early phase of renal ischemic injury.[20] In addition, the tubular epithelial cells express Bsg.[21] Accordingly, we next examined whether the difference in influx of neutrophils was mediated through differences in chemokine levels. Macrophage inflammatory protein-2 (MIP-2) and keratinocyte-derived chemokine (KC) are representative CXC chemokines that are known to be induced after ischemia/reperfusion injury and to attract neutrophils.[22] MIP-2 and KC levels were elevated in $Bsg^{+/+}$ and $Bsg^{-/-}$ mice at days 1 and 2 after ischemia/reperfusion, but there was no difference in the degree of elevation between the two genotypes (Figure 2C).

Neutrophil recruitment in the postischemia/reperfusion kidney requires adhesion molecules. E-selectin and intercellular adhesion molecule-1 (ICAM-1) on peritubular capillary cells play particularly crucial roles in this model.[23] In the present study, western blot analysis showed upregulation of E-selectin in the kidney 12 h after ischemia/reperfusion in both $Bsg^{+/+}$ and $Bsg^{-/-}$ mice, but the expression was not significantly different between the two genotypes (Figure 2D). The expression of ICAM-1 in the kidney at 24 h postischemia was also comparable between the two genotypes (Figure 2E). E-

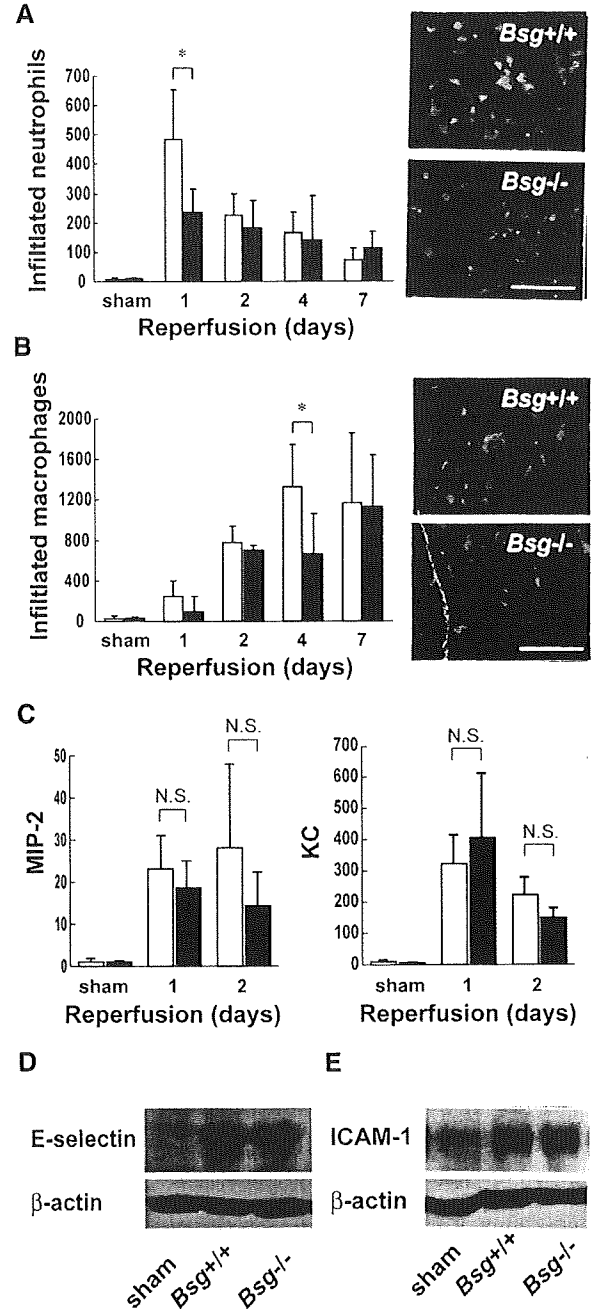

Figure 2. Reduced neutrophil influx to postischemic kidneys in $Bsg^{-/-}$ mice. (A) Neutrophil influx in postischemic kidneys. The number of infiltrated neutrophils to the kidneys after ischemia/reperfusion was counted in a blind manner. Immunostaining for neutrophils revealed suppressed influx of neutrophils into the kidneys of $Bsg^{-/-}$ compared with $Bsg^{+/+}$ mice 1 d after ischemia/reperfusion. White columns, $Bsg^{+/+}$ mice; black columns, $Bsg^{-/-}$ mice. Data are means (columns) and SEM (bars). $*P < 0.05$; $n = 6$. Representative immunostainings for neutrophils 1 d after ischemia/reperfusion are presented on the right. Scale bar, 50 μm. (B) Macrophage influx in postischemic kidneys. White columns, $Bsg^{+/+}$ mice; black columns, $Bsg^{-/-}$ mice. Data are means (columns) and SEM (bars). $*P < 0.05$; $n = 6$. Representative immunostainings for macrophages 4 d after ischemia/reperfusion are presented on the right. Scale bar, 50 μm. (C) Representative chemokine levels for neutrophil migration in the postischemic kidneys. MIP-2 and KC levels were determined by ELISA for renal homogenates and corrected for the quantity of protein. No significant differences in local MIP-2 and KC were observed between $Bsg^{+/+}$ (white columns) and $Bsg^{-/-}$ (black columns) mice. Amounts of MIP-2 and KC are presented as pg/mg protein. Data are means (columns) and SEM (bars). $n = 6$. (D) Western blot analysis of E-selectin expression in the kidney after ischemia/reperfusion. Lysates of the kidney at 12 h after ischemia/reperfusion or sham operation were subjected to immunoblot analysis of E-selectin expression. After ischemia/reperfusion injury, E-selectin expression was elevated, but the expression was comparable between the $Bsg^{+/+}$ and $Bsg^{-/-}$ mouse kidneys. (E) Western blot analysis of ICAM-1 expression in the kidney after ischemia/reperfusion. Lysates of the kidney at 24 h after ischemia/reperfusion or sham operation were subjected to immunoblot analysis. After ischemia/reperfusion injury, ICAM-1 expression was also elevated, but the expression was comparable between the $Bsg^{+/+}$ and $Bsg^{-/-}$ mouse kidneys.

selectin and ICAM-1 expression was localized along the length of the peritubular capillaries (Supplementary Figure S1).

Bsg Expression on the Surface of Neutrophils

Figure 3A shows the schematic molecular structures of Bsg and two major E-selectin ligands, PSGL-1 and CD44. Bsg is a type 1 integral membrane protein with a predicted molecular mass of 28 kD, but its glycosylated form on various cells is between 35 and 66 kD, with the actual molecular mass being dependent on the cell type.[24] Thus, highly glycosylated Bsg harbors long sugar chains. This is in contrast to PSGL-1 (approximately 120 kD) and CD44 (approximately 85 kD), which have relatively short glycans. Determinants for E-selectin-binding exist on *O*-glycans of PSGL-1 and *N*-glycans of CD44.[25,26]

The molecular mass of Bsg from peritoneal-elicited neutrophils was reduced by *N*-glycosidase F digestion as well as endo-β-glycosidase digestion, indicating that Bsg harbored *N*-linked polylactosamine chains (Figure 3B). This was consistent with a previous report.[27] We then analyzed the subcellular distribution of Bsg in neutrophils. At the electron microscope level, neutrophils display a complex surface architecture with prominent microvillus-like membrane protrusions. These microvilli represent principal sites of initial contact with the vascular endothelium. As shown in Figure 3C, a and b, Bsg was widely distributed on both the planar cell surface and the microvilli of peritoneal-elicited neutrophils. A negative control experiment was performed with an isotype-matched antibody, but no signals were observed (Figure 3Cc). The microvillous presentation argues for the participation of Bsg in the early interaction between neutrophils and endothelial cells during extravasation. Bsg may also be expressed on the surface of unstimulated neutrophils as well, since Bsg is readily detected by FACS analysis on leukocytes obtained from peripheral blood.[28]

Bsg Binds to E-Selectin

Consistent with Figure 3C, Bsg expression on the cell surface of peritoneal-elicited neutrophils was confirmed by FACS analysis, but the expression was lost in neutrophils from $Bsg^{-/-}$ mice (Figure 4A). Peritoneal-elicited neutrophils from wild-type mice bound to soluble mouse E-selectin (E-selectin/Fc) and P-selectin (P-selectin/Fc) (Figure 4B). Notably, $Bsg^{-/-}$ neutrophils showed less binding to E-selectin (Figure 4B). On the other hand, there was no difference in binding to P-selectin between $Bsg^{+/+}$ and $Bsg^{-/-}$ neutrophils (Figure 4B).

Since this result suggested that Bsg might bind to E-selectin, we next addressed this question. We examined Bsg isolated from HL-60 cells, a human promyelocytic cell line, that were pretreated with or without tunicamycin. Protein extracts from HL-60 cells were incubated with immunomagnetic beads coated with mouse anti-human Bsg antibody. Immobilized Bsg beads were then incubated with soluble human E-selectin and P-selectin with or without EDTA. Soluble E-selectin bound to the Bsg beads, and this binding was abrogated under a Ca^{2+} chelate condition (Figure 4C, left upper panel, solid line). Because it has been reported that mouse E-selectin/Fc has a higher level of binding activity to human leukocytes than human E-selectin/Fc,[29] we also used mouse E-selectin/Fc. Mouse E-selectin/Fc bound to the Bsg beads (Figure 4C, left upper panel, dotted line). On the other hand, human P-selectin/Fc did not bind to the Bsg beads (Figure 4C). Tunicamycin treatment abolished *N*-linked glycans from Bsg (Figure 4C, right) and consequently di-

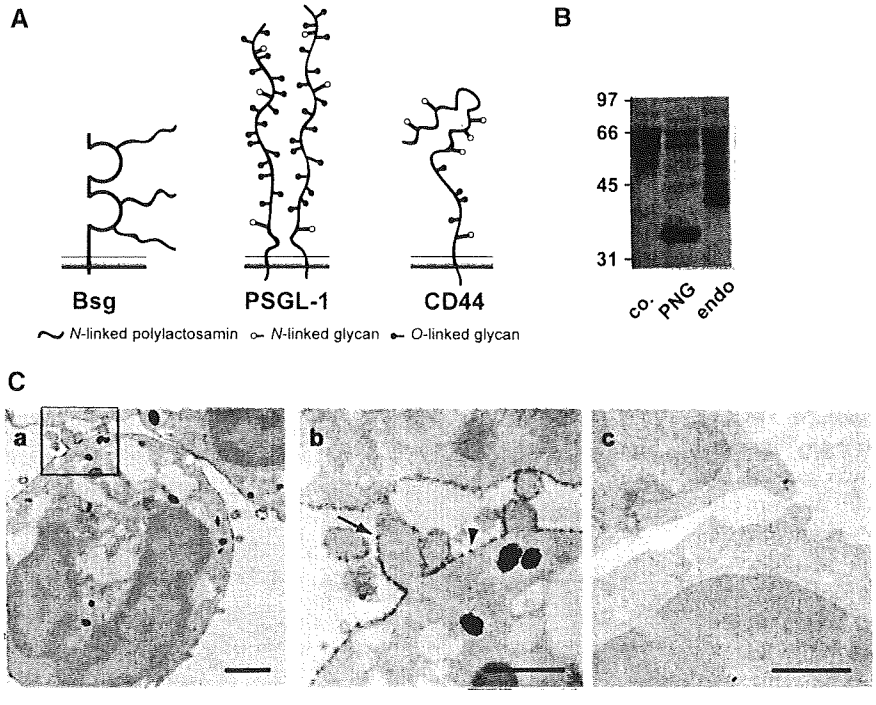

Figure 3. Bsg expression on the surface of neutrophils. (A) Structural diagrams representing Bsg, PSGL-1, and CD44. (B) Extracts from mouse neutrophils were treated with N-glycosidase F or endo-β-galactosidase and then subjected to western blot analysis. Molecular mass markers (in kD) are indicated on the left. co, untreated control; PNG, N-glycosidase F; endo, endo-β-galactosidase. (C) Immunoelectron micrograph showing the subcellular distribution of Bsg on the surface of neutrophils. Neutrophils were stained with anti-mouse Bsg antibody (a and b) or control antibody (c). The photo shown in (b) represents a magnification of the framed area in (a). Bsg was distributed both on microvilli (arrow) and on the planar surface of the neutrophils (arrowhead). Scale bars indicate 1 μm in (a) and 500 nm in (b and c).

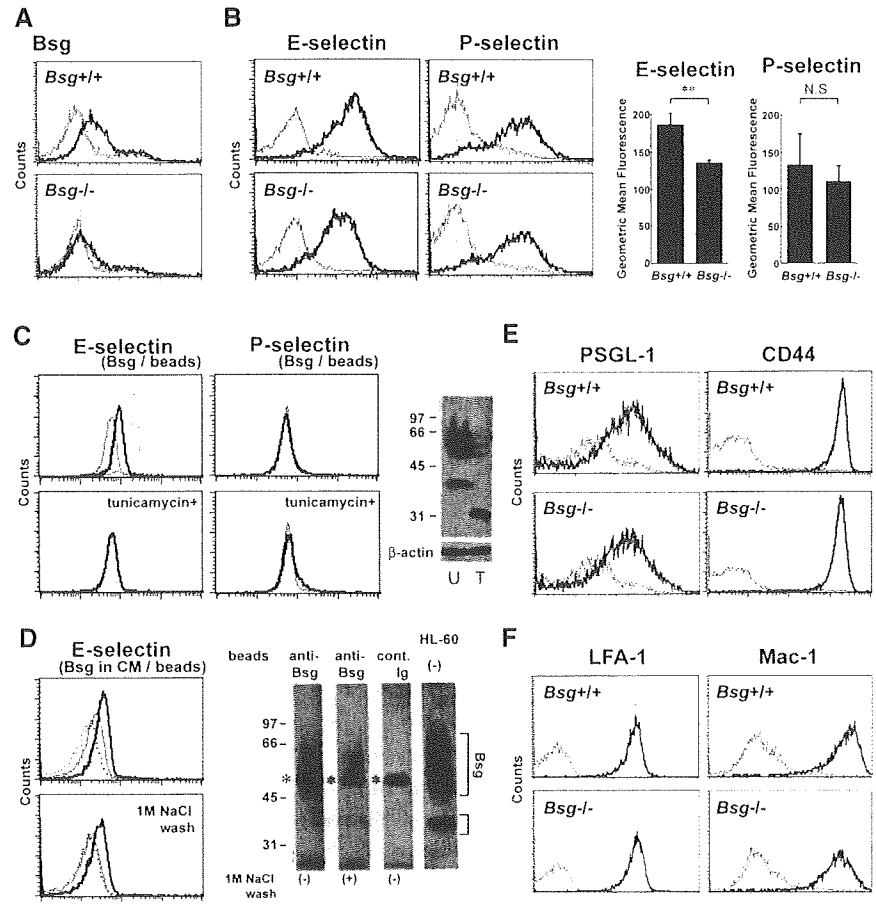

Figure 4. Neutrophil Bsg binds to E-selectin. (A) Bsg expression on mouse neutrophils. Peritoneal-elicited neutrophils were stained with anti-mouse Bsg antibodies (open histogram) or isotype-matched control antibodies (gray-filled histogram). Analysis gates were set on the granulocytic population using forward/side scatter distributions. The upper panel shows the data for $Bsg^{+/+}$ mice, and the lower one the data for $Bsg^{-/-}$ mice. (B) E-selectin and P-selectin ligands on $Bsg^{+/+}$ and $Bsg^{-/-}$ mouse neutrophils. Peritoneal-elicited neutrophils were stained with E-selectin/Fc or P-selectin/Fc. Gray-filled histograms represent EDTA treatment. The geometric mean fluorescence of E-selectin and P-selectin binding is indicated next to the histograms. Data are means (columns) and SEM (bars). $^{**}P < 0.01$; $n = 3$. (C) Binding of E-selectin and P-selectin to Bsg immunopurified from HL-60 cells. The solid lines indicate the binding of human E- or P-selectin/Fc to the beads. The dotted line indicates that of mouse E-selectin/Fc to the beads. Gray-filled histograms represent EDTA treatment. The lower panels show binding to Bsg, which was immunopurified from HL-60 cells pretreated with tunicamycin to inhibit N-glycosylation. Tunicamycin treatment abolished the binding between Bsg and E-selectin. The right panel shows western blot analysis results for Bsg and β-actin expression in tunicamycin-treated (T) or untreated (U) HL-60 cells. Molecular mass markers (in kDa) are indicated on the left. (D) Binding of E-selectin to Bsg immunopurified from HL-60 culture medium supernatant (upper panel). In the lower panel, the immunopurified beads were further washed with 1 M NaCl-PBS and then subjected to this binding assay. The solid lines indicate the binding of human E-selectin/Fc to the Bsg-coated beads. The dotted line indicates the binding to the control beads. Gray-filled histograms represent EDTA treatment. The protein(s) on the beads used in this FACS analysis were detached from the beads, and subjected to western blot analysis for Bsg (right panel). The smear bands of Bsg are indicated. Asterisks indicate the position of the heavy chain of IgG. Anti-Bsg, the beads were coated with anti-human Bsg antibody before incubating with HL-60 culture medium supernatant; cont. Ig, the beads were coated with normal mouse IgG; HL60, the lysate of HL-60 cells. Molecular mass markers (in kDa) are indicated on the left. (E) PSGL-1 and CD44 expression on $Bsg^{+/+}$ and $Bsg^{-/-}$ neutrophils. Gray-filled histograms represent the isotype-matched control. (F) Integrin expression on mouse neutrophils. Peritoneal-elicited neutrophils were stained with anti-CD11a (LFA-1) or anti-CD11b (Mac-1) antibodies (open histogram). Gray-filled histograms represent the isotype-matched control.

minished the binding between E-selectin and isolated Bsg (Figure 4C, left lower panel).

A recent study revealed that Bsg is released from the cell surface via microvesicle shedding, which is promoted by PMA.[30] As these microvesicles are unstable and rapidly broken down, Bsg can be recovered from the supernatant fraction of the culture medium after centrifugation.[30] In the present study, we treated HL-60 cells with 100 nM PMA for 24 h and detected Bsg secretion in the culture medium by western blot (data not shown). We prepared Bsg beads from this culture medium supernatant. Human E-selectin bound to these Bsg beads (Figure 4D, upper panel, solid line). Even after washing with 1 M NaCl, the beads retained the ability to bind to E-selectin, suggesting that soluble factors, if any, binding to Bsg on the beads do not affect the binding ability of the beads (Figure 4D, lower panel).

Expression of Other Adhesion-Related Molecules in Bsg-Deficient Neutrophils

The level of expression of the major E-selectin ligands PSGL-1 and CD44 on neutrophils was similar between $Bsg^{+/+}$ and $Bsg^{-/-}$ neutrophils (Figure 4E). In the renal ischemia/reperfusion injury model, integrins on the neutrophils are another factor to be considered.[31] However, we found that the expressions of lymphocyte function antigen 1 (LFA-1: CD11a/CD18) and macrophage-1 antigen (Mac-1: CD11b/CD18) on neutrophils from $Bsg^{+/+}$ mice were comparable to those on neutrophils from $Bsg^{-/-}$ mice (Figure 4F).

In addition to PSGL-1 and CD44, CD43 is known to function as an E-selectin ligand.[32] However, there was no difference of CD43 expression between $Bsg^{+/+}$ and $Bsg^{-/-}$ neutrophils (Supplementary Figure S2A). Furthermore, the beads used for Figure 4C did not contain PSGL-1, CD44, or CD43 (Supple-

mentary Figure S2B). Together with the data shown in Figure 4D, these data exclude the possibility that the Bsg used for the bead experiments was co-isolated with associated molecules that exert an E-selectin-binding activity.

Impaired $Bsg^{-/-}$ Neutrophil Adhesion to Cytokine-Activated Endothelial Cells

We next investigated the biologic significance of Bsg on neutrophils using an *in vitro* adhesion assay. It is known that human umbilical vein endothelial cells (HUVECs) express E- and P-selectin upon stimulation with TNF-α. We found that, compared with $Bsg^{+/+}$ neutrophils, $Bsg^{-/-}$ neutrophils were less adherent to HUVECs at 4 h after TNF-α stimulation (Figure 5, A and B). This result was primarily due to the interaction between E-selectin and its ligands, since an E-selectin-blocking antibody significantly suppressed the adhesion, and the difference in adherence to HUVECs between $Bsg^{+/+}$ and $Bsg^{-/-}$ neutrophils was abolished (Figure 5A). The adhesion was further suppressed when Ca^{2+} was chelated with EDTA, suggesting that, in addition to E-selectin, other components of the Ca^{2+}-dependent adhesion machinery, *e.g.*, other selectins, also played a role in this adhesion (Figure 5A). Indeed, P-selectin blocking antibody suppressed the neutrophil adhesion to HUVECs, but the difference in adhesion between the two genotypes remained intact (Figure 5B). It is noteworthy that the adhesion between HUVECs and $Bsg^{+/+}$ neutrophils was suppressed by approximately 50% by the E-selectin-blocking antibody, whereas the adhesion between HUVECs and $Bsg^{-/-}$ neutrophils was only suppressed by about 10% by this antibody (Figure 5A). Therefore, the results strongly suggested that Bsg on neutrophils played an indispensable role in adhesion to HUVECs through E-selectin.

Few Neutrophils from $Bsg^{-/-}$ Mice Infiltrated into the Postischemic Kidney

The suppressed infiltration of neutrophils in $Bsg^{-/-}$ mice after renal ischemia/reperfusion could be interpreted in two ways. First, Bsg on infiltrating neutrophils may have played a role. Second, Bsg on other cells in the inflammatory tissues may have been important. To examine these possibilities, fluorescence-labeled neutrophils were adoptively transferred into mice 5 min after renal ischemia/reperfusion surgery. After 6 h, the mice were sacrificed, and the postischemic kidneys were examined. The fluorescence-labeled neutrophils predominantly infiltrated around the vasa recta in the outer medulla, which was one of the main damaged areas after ischemia/reperfusion injury (Figure 6Aa). Much less infiltration was observed when $Bsg^{-/-}$ neutrophils were injected, compared with $Bsg^{+/+}$ neutrophils (Figure 6A, a and b, neutrophils are indicated by arrows). Labeled cells were barely detectable in the right kidney, which was not subjected to ischemia/reperfusion surgery (Figure 6Ac). Labeled cells were also not observed when saline was injected instead of labeled neutrophils (Figure 6Ad). The numbers of labeled cells infiltrating into the postischemic kidney are summarized in Figure 6B. Regardless of the genotypes of recipients, fewer adopted $Bsg^{-/-}$ neutrophils infiltrated than adopted $Bsg^{+/+}$ neutrophils. These data clearly indicated that Bsg on neutrophils, rather than Bsg on other cells at inflammatory sites, was responsible for the reduced infiltration of neutrophils into the postischemic kidney in $Bsg^{-/-}$ mice (Figure 2A). We confirmed that the infiltrating labeled cells (PKH26; Figure 6Cc, red) were indeed neutrophils by staining with anti-mouse neutrophil antibody (Figure 6Cb, green). Thus, the red and green spots were completely merged (Figure 6Ca). We also confirmed that infiltrating cells were located on the portions of the endothelium that were positive for E-selectin and thrombomodulin, a vascular endothelial marker (Figure 6C, d through i). Thus, E-selectin expression was found along the peritubular capillary blood vessels of the postischemic kidney, and the PKH26-labeled cells were in close proximity to E-selectin (Figure 6C, d through f). As the majority of the PKH26 staining in Figure 6C, c and f, represents autofluorescence, the PKH26-labeled cells are indicated by arrows in these figures.

DISCUSSION

In this study, we demonstrated that Bsg isolated from HL-60 bound to E-selectin, but not after *N*-linked polylactosamine

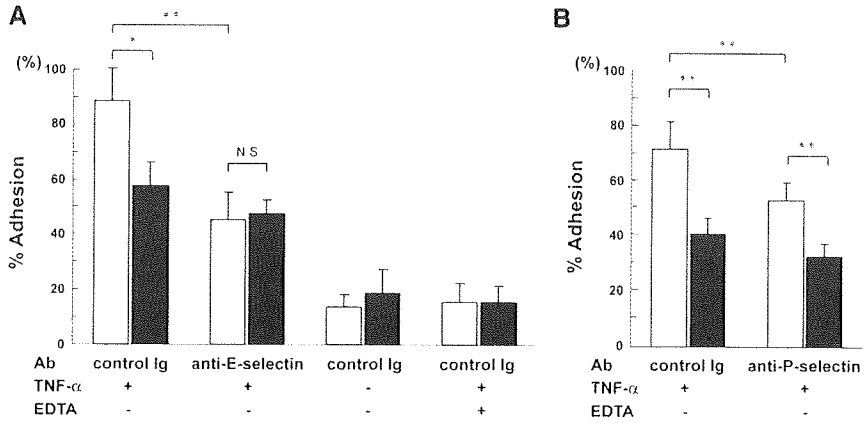

Figure 5. Adhesion assay of mouse neutrophils to HUVECs. (A) Fluorescence-labeled mouse neutrophils were incubated on TNF-α-stimulated HUVECs. Relative adhesion (% input) is shown. Control Ig, HUVECs were pretreated with isotype-matched control antibody; anti-E-selectin, HUVECs were pretreated with anti-E-selectin antibody. White columns, neutrophils from $Bsg^{+/+}$ mice; black columns, neutrophils from $Bsg^{-/-}$ mice. (B) Experiments were performed as in panel A, using anti-P-selectin antibody. anti-P-selectin, HUVECs were pretreated with anti-P-selectin antibody. Data are means (columns) and SEM (bars). $^*P < 0.05$; $^{**}P < 0.01$; $n = 5$.

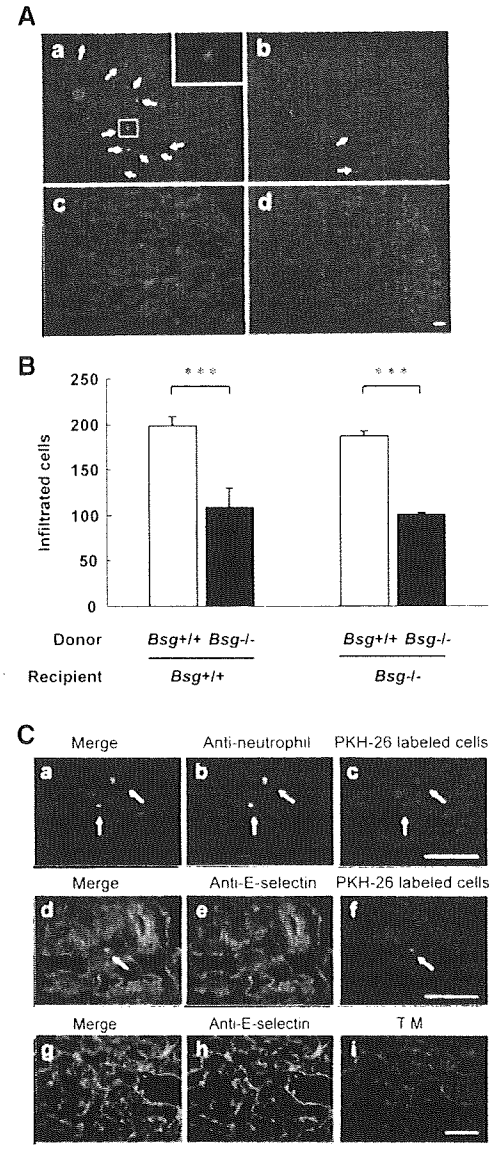

Figure 6. Adoptive transfer of neutrophils. (A) Adoptive transfer of labeled neutrophils just after renal ischemia/reperfusion. (a) $Bsg^{+/+}$ neutrophils were adoptively transferred to $Bsg^{+/+}$ recipient mice. Insert, a magnified image of the framed field. (b) $Bsg^{-/-}$ neutrophils were adoptively transferred to $Bsg^{+/+}$ recipient mice. (c) A contralateral kidney that did not receive ischemia/reperfusion. (d) A kidney that was injected with saline instead of labeled neutrophils. Arrows show labeled neutrophils. All specimens were obtained 6 h after ischemia/reperfusion. Scale bar, 100 μm. (B) The numbers of labeled (adopted) neutrophils infiltrated into the kidneys after ischemia/reperfusion. Cell counting was performed as described in the Concise Methods section. Data are means (columns) and SEM (bars). ***$P < 0.001$; $n = 3$. (C) Immunostaining of mouse neutrophils and E-selectin after adoptive transfer of labeled cells. PKH26-labeled $Bsg^{+/+}$ neutrophils (red) were adoptively transferred to $Bsg^{+/+}$ recipient mice after ischemia/reperfusion. Kidney specimens were then immunostained with anti-neutrophil antibody followed by FITC-conjugated secondary antibody (green in a through c) or by anti-E-selectin antibody followed by FITC-conjugated secondary antibody (green in d through f). The arrows indicate fluorescence-positive cells. The capillary endothelium was also stained with anti-thrombomodulin (TM) antibody followed by rhodamine-conjugated secondary antibody (g through i). Scale bar, 50 μm.

chains of Bsg were ablated by tunicamycin treatment. The massive neutrophil infiltration into the kidney after renal ischemia/reperfusion was partly attributable to Bsg on neutrophils, because (*i*) the level of neutrophil infiltration was lower in $Bsg^{-/-}$ mice and (*ii*) regardless of the recipients' genotypes, exogenously injected $Bsg^{-/-}$ neutrophils were less readily recruited to the inflammatory kidney tissue. *In vitro* E-selectin-dependent adherence to HUVECs was also reduced in $Bsg^{-/-}$ neutrophils. Therefore, our data strongly suggest that Bsg is a physiologic ligand for E-selectin.

The selectins are required for leukocyte adhesion during inflammation. E-selectin but not P-selectin controls slow leukocyte rolling on inflamed venules, and this rolling may enhance an efficient transition to firm adhesion and extravasation.[33–35] Although blocking of P-selectin ameliorates ischemia/reperfusion-induced AKI, platelet P-selectin, but not endothelial P-selectin, is the key component in P-selectin-mediated AKI.[36,37] Therefore, we focused on endothelial E-selectin and its ligand in these renal ischemia/reperfusion experiments. Several glycoproteins have been found to bind to E-selectin *in vitro*, and the topographic distribution of the ligands on the surface of neutrophils is a major determinant of their ability to mediate initial contacts to the endothelium under flow. For example, PSGL-1 distributes on the very tip of neutrophil microvilli and contributes to the primary interaction between neutrophils and the endothelium.[38] On the other hand, CD44 is exclusively distributed on the planar surface of the neutrophils and mediates steady slow rolling.[39] In this context, it is of note that Bsg is equally distributed on the planar surface and microvilli of the neutrophils (Figure 3C). The localization of Bsg on microvilli is an indication of its possible role in the early steps of leukocyte endothelial contact formation.

Bsg is known to induce MMPs and thus, is referred to as an extracellular matrix metalloproteinase inducer (EMMPRIN). To confirm the effects of MMP activity in the postischemic kidneys on this model, we performed gelatin zymography. Both MMP-2 and MMP-9 activities in $Bsg^{+/+}$ mice were comparable to those in $Bsg^{-/-}$ mice at both 1 and 2 d postischemia/reperfusion (data not shown). Another molecule we considered was cyclophilin. It has been reported that extracellular cyclophilins can induce leukocyte chemotaxis, and Bsg is a signaling receptor for these proteins. Blocking the cyclophilin-Bsg interaction pharmacologically or by means of an antibody reduces the inflammation responses in a LPS-induced acute lung injury model and a bronchial asthma model in mice.[28,40] Dear *et al.*[41] found that cyclophilin is upregulated in the liver in a sepsis model, and inhibition of Bsg attenuates sepsis-induced AKI.

However, the expression of cyclophilin A, the most representative cyclophilin, did not increase after ischemia in the kidney, and there was no difference in the expression of cyclophilin A between the two genotypes in the present study (data not shown). Thus, it is not likely that the function of Bsg is always exerted through cyclophilin in AKI, although further studies are needed to fully understand the involvement of cyclophilin in AKI. Furthermore, $Bsg^{-/-}$ neutrophils expressed normal levels of PSGL-1, CD44, and integrins (LFA-1 and Mac-1). We also observed that the expression of E-selectin on renal microvessels and chemokines in the kidney was comparable between $Bsg^{+/+}$ and $Bsg^{-/-}$ mice. These data support the idea that the difference in renal damage between $Bsg^{+/+}$ and $Bsg^{-/-}$ mice was due to the difference in neutrophil infiltration mediated by Bsg on neutrophils.

Bsg on neutrophils has long sugar chains that are *N*-linked polylactosamines (Figure 3A). The biologic significance of these long sugar chains has long been obscure. In this context, it is noteworthy that *O*-linked glycans on PSGL-1 contribute to binding to its receptors, E- and P-selectins, while *N*-linked glycans on CD44 are responsible for the binding to E-selectin (Figure 3A).[8,25] Based on the present results, Bsg has unique sugar chains, *i.e.*, *N*-linked polylactosamines, that are responsible for its binding to E-selectin.

Renal ischemia/reperfusion leads to increased endothelial expression of a variety of adhesion molecules that promote endothelial-leukocyte interaction. Gene knockout, antibody, and pharmacologic inhibitor studies have suggested a role for E-selectin in ischemia/reperfusion injury.[42] In particular, E-selectin-deficient mice show a 75% reduction in myeloperoxidase activity (an indicator of neutrophil infiltration) in the postischemic kidneys at 24 h compared with wild-type mice.[23] Our $Bsg^{-/-}$ mice showed a 50% reduction in neutrophil counts in the kidney compared with wild-type mice. Therefore, Bsg may not fully account for the function of E-selectin. Our *in vitro* binding assay between neutrophils and HUVECs also supports this idea. Therefore, other E-selectin ligands on neutrophils, such as PSGL-1 and CD44, may also be important for neutrophil recruitment and the subsequent renal damages induced by ischemia/reperfusion. Infiltrating neutrophils produce cytokines, growth factors, proteases, and reactive oxygen species, all of which can injure renal cells. Injured renal cells in turn produce factors that stimulate neutrophils. This chain reaction may contribute to the establishment of renal dysfunction. If neutrophil infiltration is moderately suppressed as in the case of $Bsg^{-/-}$ mice, the suppression of renal dysfunction may be delayed. Therefore, the delayed effect of Bsg deficiency on BUN as compared with E-selectin knockout may not necessarily indicate that Bsg is not an early-acting E-selectin ligand. Rather, the localization of Bsg on the microvilli (Figure 3) may suggest that it participates in initial capture (tethering) on the endothelium, as in the case of PSGL-1.[7]

Finally, our study has shed light on the mechanisms underlying AKI. There is no specific therapy for AKI except for supportive care, and AKI is associated with unacceptably high mortality that has been reported to range from 40% to 60%.[17,43] The overwhelming majority of studies have exclusively looked at neutrophils as the most important prevalent leukocytes during AKI. Our study thus introduces a novel player in the pathogenesis of AKI. Bsg might be a good candidate target for intervention of AKI.

CONCISE METHODS

Bsg-Deficient Mice

Mice deficient in the *Bsg* gene were generated as described previously.[44] All experiments were performed with $Bsg^{+/+}$ and $Bsg^{-/-}$ littermates. The mice used were 8- to 12-wk-old females weighing 20 to 25 g. The mice were housed under controlled environmental conditions and maintained with standard food and water.

The experiments described above were conducted according to The Animal Experimentation Guide of Nagoya University School of Medicine.

Renal Ischemia/Reperfusion Injury Model

We used a previously characterized model of renal ischemia/reperfusion injury in mice.[45] Briefly, we anesthetized the mice by intraperitoneal administration of 40 mg/kg sodium pentobarbital. We placed the animals on a heating pad to maintain a constant body temperature of 37°C. Under general anesthesia, we removed the right kidney. This heminephrectomy procedure was omitted in the experiment of adoptive transfer of labeled neutrophils. After 7 d, we anesthetized the mice as described above and exposed the left kidney. We occluded the renal artery for 45 min with nontraumatic microvascular clamps. The animals received 30 ml/kg warm saline instilled into the peritoneal cavity after the procedure and were allowed to recover with free access to food and water. Sham-operated mice underwent the same procedure without clamping of the artery and were killed 1 d after surgery. Groups of mice ($n = 6$) were killed 1, 2, 4, and 7 d after surgery.

We determined serum urea by a standard diagnostic procedure using a kit from KAINOS Laboratories (Tokyo, Japan).

We measured the cytokine MIP-2 and KC in renal homogenates as described previously[46] by specific ELISA according to the manufacturer's instructions (MIP-2: R&D Systems; KC: Immuno-Biologic Laboratories Ltd., Gunma, Japan). We normalized the results for the total protein concentration.

Histology

We fixed renal tissues in 4% paraformaldehyde, embedded them in paraffin, and then cut them into 2-μm sections. We stained the sections with periodic acid-Schiff reagent. Using semiquantitative indices, we analyzed the sections to evaluate tubulointerstitial damage in each region by light microscopy, as described previously.[45] Briefly, the extent of cast formation, tubular dilation, and tubular degeneration in the cortex, outer medulla, and inner medulla were scored according to the fol-

lowing criteria by two observers in a blind manner: 0, normal; 1, below 30% of the pertinent area; 2, 30% to 70% of the pertinent area; 3, over 70% of the pertinent area.

Parts of the kidney tissues were snap-frozen in liquid nitrogen. We cut 2-μm-thick sections with a cryostat and then fixed them in acetone. We stained the cryosections with rat anti-mouse neutrophil antibody (dilution, 1:200; clone 7/4; Serotec, Oxford, UK), rat anti-mouse macrophage antibody (dilution, 1:50; clone F4/80; Serotec), rat anti-mouse E-selectin antibody (dilution, 1:50; clone 96419; R&D Systems, Minneapolis, MN), or goat anti-mouse ICAM-1 antibody (dilution, 1:50; R&D Systems), followed by detection with FITC-conjugated rabbit anti-rat IgG (dilution, 1:100; Zymed Laboratories, San Francisco, CA) or FITC-conjugated rabbit anti-goat IgG (dilution, 1:100; Sigma-Aldrich, St. Louis, MO). We counted leukocytes positive for 7/4 and F4/80 in all renal regions (cortex, outer medulla, and inner medulla) under a microscope at $\times$200 magnification in a blind manner.

For immunoelectron microscopy, we washed peritoneal-elicited mouse neutrophils twice and then stained them with rat anti-mouse Bsg antibody (dilution, 1:25; clone OX114; Abcam Ltd., Cambridge, UK) or control rat IgG followed by HRP-conjugated goat F(ab')$_2$ fragment anti-rat IgG (Histofine; Nichirei Corporation, Tokyo, Japan). After fixation with 1% glutaraldehyde, we incubated the cells with 3,3' diaminobenzidine (Dako, Carpinteria, CA) for 30 min, then washed them twice. The cells were postfixed in osmium tetroxide, dehydrated in alcohol, and embedded in epoxy resin (Quetol-812; Nissin EM Corporation, Tokyo, Japan). We examined ultrathin sections with a JEM-1400 electron microscope (JOEL Ltd., Tokyo, Japan).

Preparation of Mouse Peritoneal-Elicited Neutrophils

Mouse peritoneal neutrophils were elicited by intraperitoneal injection of 2 ml 3% thioglycollate medium (Wako, Osaka, Japan), which induced aseptic peritoneal inflammation. After 5 h, we collected peritoneal exudate fluid with 5 ml ice-cold PBS.[47] We washed the isolated peritoneal cells three times. The purity of neutrophils was approximately 90% as confirmed by FACS analysis (anti-GR-1-positive cells) and May-Giemsa staining. The cell viability was more than 98% checked by trypan blue staining.

Cells

HUVECs (Cell Applications, San Diego, CA) were cultured using an EGM-2 BulletKit (Takara Bio, Shiga, Japan) at 37°C in 5% CO_2 and used between the second and fifth passages. We obtained the human promyelocytic cell line HL-60 from the American Type Culture Collection (ATCC; accession no. CCL-240; Manassas, VA) and cultured them in RPMI 1640 (Sigma-Aldrich) containing 10% fetal bovine serum (Life Technologies BRL, Gaithersburg, MD) at 37°C in 5% CO_2.

Deglycosylation

To remove *N*-glycans in the cell lysate, we treated the lysate of mouse peritoneal-elicited neutrophils with 10 U N-glycosidase F (Roche Diagnostics, Mannheim, Germany) at 37°C overnight in a buffer containing 50 mM sodium phosphate, pH 7.5, and 1% Nonidet-P 40. To remove polylactosamine chains in the cell lysate, we treated the cell lysate with 5 mU endo-β-galactosidase (Seikagaku Corporation, Tokyo, Japan) at 37°C overnight in a buffer containing 10 mM sodium acetate, pH 6.0.

For the inhibition of *N*-glycosylation in cells, we cultured HL-60 cells in the presence of 15 μg/ml tunicamycin (Calbiochem, San Diego, CA) for 48 h.

Flow Cytometry E- and P-Selectin-Binding Assay

First, we prepared immunomagnetic beads. Lysates were prepared by incubation of HL-60 in lysis buffer (1% Triton-X 100 in PBS with EDTA-free Protease Inhibitor Cocktail; Nakalai Tesque, Kyoto, Japan) for 30 min on ice, and cell debris was removed by centrifugation at 17,000 $\times$ *g* for 10 min at 4°C. We incubated anti-mouse IgG-coated beads (M-280 Dynabeads; Dynal Biotech ASA, Oslo, Norway) with mouse anti-human Bsg antibody (clone MEM-M6/1; Abcam Ltd.) and control mouse IgG for 4 h under rotation. We then washed the beads twice with lysis buffer and incubated them overnight at 4°C under rotation with the prepared HL-60 cell lysate (2×10^6 cells/10^6 beads) or culture medium supernatant obtained after ultracentrifuge. We washed the beads three times with PBS or 1 M NaCl-PBS before the binding assay. To detach the protein on the prepared immunomagnetic beads, we boiled the beads with sample buffer for 5 min. We then subjected the supernatants to western blot analysis.

Mouse peritoneal-elicited neutrophils (5×10^5) were stained by incubation with antibody against Bsg (dilution, 1:50; clone OX114; Abcam Ltd.), PSGL-1 (dilution, 1:50; clone 4RA10; Becton Dickinson, Franklin Lakes, NJ), CD44 (dilution, 1:50; IM7; BioLegend, San Diego, CA), CD11a (dilution, 1:50; clone I21/7; SouternBiotech, Birmingham, AL), CD11b (dilution, 1:50; clone M1/70; Cedarlane, ON, Canada), Gr-1 (dilution, 1:100; clone RB6–8C5; Cedarlane), and CD43 (dilution, 1:50; clone 1B11; Biolegend) or control antibodies. Subsequently, we washed these cells with PBS and then incubated them with FITC-conjugated anti-rat IgG (dilution, 1:100; Zymed Laboratories). Cells were washed three times before flow cytometry analysis. To assess the E- and P-selectin-binding property, we incubated mouse peritoneal-elicited neutrophils or prepared Bsg-coated beads with 10 μg/ml recombinant human E-selectin/Fc chimera, human P-selectin/Fc chimera, mouse E-selectin/Fc chimera, and mouse P-selectin/Fc chimera (R&D Systems) at 4°C with gentle shaking for 30 min in the presence or absence of 5 mM EDTA. We then incubated the cells with FITC-conjugated goat F(ab')$_2$ fragment anti-human IgG (Fcγ; Beckman Coulter, Fullerton, CA). In the analysis of mouse neutrophils, the gates were set on the granulocytic population using forward/side scatter distributions. All samples were analyzed using a FACSCalibur flow cytometer and CellQuest software (Becton Dickinson).

Western Blot Analysis

We performed western blot analysis as described previously.[48] Briefly, we separated the samples by 10% SDS-PAGE and then transferred the gels to a nitrocellulose membrane (Whatman, Florham Park, NJ). We blocked the membranes with 5% (wt/vol) dry fat-free milk in PBS with 0.1% Tween for 60 min at room temperature. We then incubated the membranes with rat anti-mouse E-selectin antibody (dilution, 1:1000; clone 96419; R&D Systems), goat anti-mouse ICAM-1 antibody (dilution, 1:1000; R&D Systems), goat anti-mouse Bsg antibody (dilution, 1:1000; R&D Systems), mouse anti-human Bsg antibody (dilution, 1:1000; clone HIM6; Biolegend), mouse anti-human PSGL-1 antibody (dilution, 1:1000; clone KPL-1; BD Biosciences), mouse anti-human CD44 antibody (dilution, 1:1000; clone 2C5; R&D Systems), mouse anti-human CD43 antibody (dilution, 1:1000; clone MEM-59; Biolegend), rabbit anti-mouse cyclophilin A antibody (dilution, 1:1000; Upstate, Lake Placid, NY), or mouse anti-β actin antibody (dilution, 1:1000; Sigma-Aldrich). Each primary antibody was incubated at 4°C overnight. After washing with PBS containing 0.1% Tween, we incubated these membranes with peroxidase-conjugated anti-rat IgG, anti-goat IgG, or anti-mouse IgG (dilution, 1:5000; Jackson Immunoresearch Laboratories, West Grove, PA), respectively, for 60 min at room temperature. We visualized the proteins with an enhanced chemiluminescence (ECL) detection system (Amersham Pharmacia, Amersham Biosciences, Piscataway, NJ).

Adhesion Assay of Mouse Neutrophils to HUVECs

We performed the adhesion assay on HUVECs as described previously.[49] Briefly, we washed the mouse peritoneal-elicited neutrophils in HBSS without Ca^{2+} and Mg^{2+} and concentrated them to 10^7 cells/ml. We then incubated the suspensions with 5 μM calcein-AM (Molecular Probes, Eugene, OR) at 37°C for 15 min.[50] We stopped the labeling by adding RPMI 1640 with 10% fetal bovine serum and washing three times. HUVECs were plated at 5×10^4 cells/well in a 96-well microplate (MICROTEST 96; Becton Dickinson). After overnight culture, we obtained confluent monolayers. To stimulate the expression of endothelial adhesion molecules, including E-selectin, we pretreated HUVECs with 10 ng/ml recombinant human TNF-α (R&D Systems) for 4 h at 37°C. Afterwards, HUVECs were washed twice and then treated with 30 μg/ml rat anti-human CD62E (E-selectin) antibody (clone UZ4; Abcam Ltd.), 20 μg/ml sheep anti-human CD62P (P-selectin) antibody (R&D Systems), control rat antibody (clone RTK2118; Abcam Ltd.), or control sheep antibody (Santa Cruz Biotechnology, Santa Cruz, CA) for 1 h. After washing, we allowed 5×10^5 fluorescence-labeled mouse neutrophils in RPMI 1640 medium to adhere for 30 min with or without EDTA. This procedure was examined at 4°C, since this temperature is known to be optimal for the investigation of the selectin-mediated adhesion mechanism and does not activate integrins.[51]We then inverted the plates for 30 min to eliminate unadherent cells and washed carefully. We then added an equal number of labeled cells (5×10^5) to the well to measure total fluorescence (F_t). The remaining fluorescence (F_x) and the fluorescence of a blank well (F_b) were measured.[50] We measured all fluorescences on a Fluoroskan AscentCF (Labsystems, Helsinki, Finland). Calcein-AM-labeled cells were excited at 485 nm and evaluated at 530 nm. We calculated the percentage adhesion using the following formula:

$$\%\text{adhesion} = \frac{F_x - F_b}{F_t - F_b} \times 100.$$

Adoptive Transfer of Labeled Neutrophils

We washed peritoneal-elicited neutrophils from $Bsg^{+/+}$ and $Bsg^{-/-}$ mice with PBS and stained them with a PKH26 red fluorescence cell linker kit (Sigma-Aldrich) according to the manufacturer's instructions. The viability of neutrophils was more than 98% after labeling with trypan blue exclusion. Five million neutrophils from $Bsg^{+/+}$ and $Bsg^{-/-}$ mice were injected intravenously into $Bsg^{+/+}$ and $Bsg^{-/-}$ mice, respectively, at 5 min after renal ischemia/reperfusion surgery. After 6 h of reperfusion, we harvested the postischemic kidney. We prepared frozen sections of the kidney at 4-μm thickness. We counted the number of transferred neutrophils (PKH26-labeled cells) by examining all renal regions in 20 continuous sections of the short axis hilum of the kidney. Then we fixed other sections as described above and stained them with rat anti-mouse neutrophil antibody (clone 7/4; Serotec), followed by FITC-conjugated rabbit anti-rat IgG (Zymed Laboratories) to confirm that the infiltrated PKH26-labeled cells were neutrophils. We incubated other sections with chicken anti-mouse E-selectin antibody (dilution, 1:50; R&D Systems), followed by FITC-conjugated rabbit anti-chicken IgG (dilution, 1:50; Zymed Laboratories) to check the positional relations of transferred neutrophils in the kidney. For double-immunofluorescence staining of E-selectin and the endothelium, we first stained the section with E-selectin as described above. It was then incubated with rabbit anti-rat thrombomodulin antibody[52] (dilution, 1:1000) followed by incubation with rhodamine-conjugated goat anti-rabbit IgG (dilution, 1:100; Zymed Laboratories).

Statistical Analysis

We expressed all values as means ± SEM. We performed statistical analysis with unpaired, two-tailed t test for single comparisons. Values of $P < 0.05$ were considered to indicate statistically significant differences.

ACKNOWLEDGMENTS

We thank Kenji Uchimura for his helpful comments on this manuscript and Norihiko Suzuki, Naoko Asano, and Yuriko Sawa for their excellent technical assistance. This work was supported by a Grant-in-Aid from the Ministry of Education, Science, Sports, and Culture of Japan (no. 19590947 to Y.Y.)

DISCLOSURES

None.

REFERENCES

1. Ley K: The role of selectins in inflammation and disease. *Trends Mol Med* 9: 263–268, 2003
2. Vestweber D, Blanks JE: Mechanisms that regulate the function of the selectins and their ligands. *Physiol Rev* 79: 181–213, 1999
3. Sperandio M, Smith ML, Forlow SB, Olson TS, Xia L, McEver RP, Ley K: P-selectin glycoprotein ligand-1 mediates L-selectin-dependent leukocyte rolling in venules. *J Exp Med* 197: 1355–1363, 2003
4. Bullard DC, Kunkel EJ, Kubo H, Hicks MJ, Lorenzo I, Doyle NA, Doerschuk CM, Ley K, Beaudet AL: Infectious susceptibility and severe deficiency of leukocyte rolling and recruitment in E-selectin and P-selectin double mutant mice. *J Exp Med* 183: 2329–2336, 1996
5. Frenette PS, Mayadas TN, Rayburn H, Hynes RO, Wagner DD: Susceptibility to infection and altered hematopoiesis in mice deficient in both P- and E-selectins. *Cell* 84: 563–574, 1996
6. Labow MA, Norton CR, Rumberger JM, Lombard-Gillooly KM, Shuster DJ, Hubbard J, Bertko R, Knaack PA, Terry RW, Harbison ML, Kontgen F, Stewart CL, McIntyre KW, Will PC, Burns DK, Wolitzky BA: Characterization of E-selectin-deficient mice: Demonstration of overlapping function of the endothelial selectins. *Immunity* 1: 709–720, 1994
7. Hidalgo A, Peired AJ, Wild MK, Vestweber D, Frenette PS: Complete identification of E-selectin ligands on neutrophils reveals distinct functions of PSGL-1, ESL-1, and CD44. *Immunity* 26: 477–489, 2007
8. Lowe JB: Glycan-dependent leukocyte adhesion and recruitment in inflammation. *Curr Opin Cell Biol* 15: 531–538, 2003
9. Zarbock A, Ley K: Mechanisms and consequences of neutrophil interaction with the endothelium. *Am J Pathol* 172: 1–7, 2008
10. Miyauchi T, Kanekura T, Yamaoka A, Ozawa M, Miyazawa S, Muramatsu T: Basigin, a new, broadly distributed member of the immunoglobulin superfamily, has strong homology with both the immunoglobulin V domain and the beta-chain of major histocompatibility complex class II antigen. *J Biochem* 107: 316–323, 1990
11. Igakura T, Kadomatsu K, Kaname T, Muramatsu H, Fan QW, Miyauchi T, Toyama Y, Kuno N, Yuasa S, Takahashi M, Senda T, Taguchi O, Yamamura K, Arimura K, Muramatsu T: A null mutation in basigin, an immunoglobulin superfamily member, indicates its important roles in peri-implantation development and spermatogenesis. *Dev Biol* 194: 152–165, 1998
12. Igakura T, Kadomatsu K, Taguchi O, Muramatsu H, Kaname T, Miyauchi T, Yamamura K, Arimura K, Muramatsu T: Roles of basigin, a member of the immunoglobulin superfamily, in behavior as to an irritating odor, lymphocyte response, and blood-brain barrier. *Biochem Biophys Res Commun* 224: 33–36, 1996
13. Naruhashi K, Kadomatsu K, Igakura T, Fan QW, Kuno N, Muramatsu H, Miyauchi T, Hasegawa T, Itoh A, Muramatsu T, Nabeshima T: Abnormalities of sensory and memory functions in mice lacking Bsg gene. *Biochem Biophys Res Commun* 236: 733–737, 1997
14. Biswas C, Zhang Y, DeCastro R, Guo H, Nakamura T, Kataoka H, Nabeshima K: The human tumor cell-derived collagenase stimulatory factor (renamed EMMPRIN) is a member of the immunoglobulin superfamily. *Cancer Res* 55: 434–439, 1995
15. Kirk P, Wilson MC, Heddle C, Brown MH, Barclay AN, Halestrap AP: CD147 is tightly associated with lactate transporters MCT1 and MCT4 and facilitates their cell surface expression. *EMBO J* 19: 3896–3904, 2000
16. Philp NJ, Wang D, Yoon H, Hjelmeland LM: Polarized expression of monocarboxylate transporters in human retinal pigment epithelium and ARPE-19 cells. *Invest Ophthalmol Vis Sci* 44: 1716–1721, 2003
17. Ympa YP, Sakr Y, Reinhart K, Vincent JL: Has mortality from acute renal failure decreased? A systematic review of the literature. *Am J Med* 118: 827–832, 2005
18. Singbartl K, Ley K: Leukocyte recruitment and acute renal failure. *J Mol Med* 82: 91–101, 2004
19. Johnson KJ, Weinberg JM: Postischemic renal injury due to oxygen radicals. *Curr Opin Nephrol Hypertens* 2: 625–635, 1993
20. Abuelo JG: Normotensive ischemic acute renal failure. *N Engl J Med* 357: 797–805, 2007
21. Deora AA, Philp N, Hu J, Bok D, Rodriguez-Boulan E: Mechanisms regulating tissue-specific polarity of monocarboxylate transporters and their chaperone CD147 in kidney and retinal epithelia. *Proc Natl Acad Sci U S A* 102: 16245–16250, 2005
22. Miura M, Fu X, Zhang QW, Remick DG, Fairchild RL: Neutralization of Gro alpha and macrophage inflammatory protein-2 attenuates renal ischemia/reperfusion injury. *Am J Pathol* 159: 2137–2145, 2001
23. Singbartl K, Ley K: Protection from ischemia-reperfusion induced severe acute renal failure by blocking E-selectin. *Crit Care Med* 28: 2507–2514, 2000
24. Muramatsu T, Miyauchi T: Basigin (CD147): A multifunctional transmembrane protein involved in reproduction, neural function, inflammation and tumor invasion. *Histol Histopathol* 18: 981–987, 2003
25. Katayama Y, Hidalgo A, Chang J, Peired A, Frenette PS: CD44 is a physiological E-selectin ligand on neutrophils. *J Exp Med* 201: 1183–1189, 2005
26. Zou X, Shinde Patil VR, Dagia NM, Smith LA, Wargo MJ, Interliggi KA, Lloyd CM, Tees DF, Walcheck B, Lawrence MB, Goetz DJ: PSGL-1 derived from human neutrophils is a high-efficiency ligand for endothelium-expressed E-selectin under flow. *Am J Physiol Cell Physiol* 289: C415–C424, 2005
27. Tang W, Chang SB, Hemler ME: Links between CD147 function, glycosylation, and caveolin-1. *Mol Biol Cell* 15: 4043–4050, 2004
28. Arora K, Gwinn WM, Bower MA, Watson A, Okwumabua I, MacDonald HR, Bukrinsky MI, Constant SL: Extracellular cyclophilins contribute to the regulation of inflammatory responses. *J Immunol* 175: 517–522, 2005
29. Ni Z, Walcheck B: Varied levels of reactivity by different E-selectin/Fc constructs with cutaneous lymphocyte-associated antigen (CLA)(+) CD4(+) T cells. *Immunol Lett* 108: 179–182, 2007
30. Sidhu SS, Mengistab AT, Tauscher AN, LaVail J, Basbaum, C: The microvesicle as a vehicle for EMMPRIN in tumor-stromal interactions. *Oncogene* 23: 956–963, 2004
31. Rabb H, Mendiola CC, Dietz J, Saba SR, Issekutz TB, Abanilla F, Bonventre JV, Ramirez G: Role of CD11a and CD11b in ischemic acute renal failure in rats. *Am J Physiol* 267: F1052–F1058, 1994
32. Khunkaewla P, Schiller HB, Paster W, Leksa V, Cermak L, Andera L, Horejsi V, Stockinger H: LFA-1-mediated leukocyte adhesion regulated by interaction of CD43 with LFA-1 and CD147. *Mol Immunol* 45: 1703–1711, 2008
33. Jung U, Norman KE, Scharffetter-Kochanek K, Beaudet AL, Ley K: Transit time of leukocytes rolling through venules controls cytokine-induced inflammatory cell recruitment in vivo. *J Clin Invest* 102: 1526–1533, 1998
34. Kunkel EJ, Ley K: Distinct phenotype of E-selectin-deficient mice. E-selectin is required for slow leukocyte rolling in vivo. *Circ Res* 79: 1196–1204, 1996
35. Ley K, Allietta M, Bullard DC, Morgan S: Importance of E-selectin for firm leukocyte adhesion in vivo. *Circ Res* 83: 287–294, 1998
36. Singbartl K, Forlow SB, Ley, K: Platelet, but not endothelial, P-selectin is critical for neutrophil-mediated acute postischemic renal failure. *FASEB J* 15: 2337–2344, 2001
37. Singbartl K, Green SA, Ley K: Blocking P-selectin protects from ischemia/reperfusion-induced acute renal failure. *FASEB J* 14: 48–54, 2000
38. Moore KL, Patel KD, Bruehl RE, Li F, Johnson DA, Lichenstein HS, Cummings RD, Bainton DF, McEver RP: P-selectin glycoprotein ligand-1 mediates rolling of human neutrophils on P-selectin. *J Cell Biol* 128: 661–671, 1995
39. von Andrian UH, Hasslen SR, Nelson RD, Erlandsen SL, Butcher EC: A central role for microvillous receptor presentation in leukocyte adhesion under flow. *Cell* 82: 989–999, 1995

40. Gwinn WM, Damsker JM, Falahati R, Okwumabua I, Kelly-Welch A, Keegan AD, Vanpouille C, Lee JJ, Dent LA, Leitenberg D, Bukrinsky MI, Constant SL: Novel approach to inhibit asthma-mediated lung inflammation using anti-CD147 intervention. *J Immunol* 177: 4870–4879, 2006
41. Dear JW, Leelahavanichkul A, Aponte A, Hu X, Constant SL, Hewitt SM, Yuen PS, Star RA: Liver proteomics for therapeutic drug discovery: Inhibition of the cyclophilin receptor CD147 attenuates sepsis-induced acute renal failure. *Crit Care Med* 35: 2319–2328, 2007
42. Nemoto T, Burne MJ, Daniels F, O'Donnell MP, Crosson J, Berens K, Issekutz A, Kasiske BL, Keane WF, Rabb H: Small molecule selectin ligand inhibition improves outcome in ischemic acute renal failure. *Kidney Int* 60: 2205–2214, 2001
43. Star RA: Treatment of acute renal failure. *Kidney Int* 54: 1817–1831, 1998
44. Chen S, Kadomatsu K, Kondo M, Toyama Y, Toshimori K, Ueno S, Miyake Y, Muramatsu T: Effects of flanking genes on the phenotypes of mice deficient in basigin/CD147. *Biochem Biophys Res Commun* 324: 147–153, 2004
45. Sato W, Kadomatsu K, Yuzawa Y, Muramatsu H, Hotta N, Matsuo S, Muramatsu T: Midkine is involved in neutrophil infiltration into the tubulointerstitium in ischemic renal injury. *J Immunol* 167: 3463–3469, 2001
46. Rouschop KM, Sewnath ME, Claessen N, Roelofs JJ, Hoedemaeker I, van der Neut R, Aten J, Pals ST, Weening JJ, Florquin S: CD44 deficiency increases tubular damage but reduces renal fibrosis in obstructive nephropathy. *J Am Soc Nephrol* 15: 674–686, 2004
47. Lagasse E, Weissman IL: Flow cytometric identification of murine neutrophils and monocytes. *J Immunol Methods* 197: 139–150, 1996
48. Kadomatsu K, Hagihara M, Akhter S, Fan QW, Muramatsu H, Muramatsu T: Midkine induces the transformation of NIH3T3 cells. *Br J Cancer* 75: 354–359, 1997
49. Hisano T, Namba T, Hashiguchi-Ikeda M, Ito T, Hirota K, Fukuda K: Inhibition of E-selectin-mediated leukocyte adhesion by volatile anesthetics in a static condition. *J Anesth* 19: 1–6, 2005
50. De Clerck LS, Bridts CH, Mertens AM, Moens MM, Stevens WJ: Use of fluorescent dyes in the determination of adherence of human leucocytes to endothelial cells and the effect of fluorochromes on cellular function. *J Immunol Methods* 172: 115–124, 1994
51. Hammel M, Weitz-Schmidt G, Krause A, Moll T, Vestweber D, Zerwes HG, Hallmann R: Species-specific and conserved epitopes on mouse and human E-selectin important for leukocyte adhesion. *Exp Cell Res* 269: 266–274, 2001
52. Yuzawa Y, Brentjens JR, Brett J, Caldwell PR, Esposito C, Fukatsu A, Godman G, Stern D, Andres G: Antibody-mediated redistribution and shedding of endothelial antigens in the rabbit. *J Immunol* 150: 5633–5646, 1993

Int. J. Cancer: **125**, 2978–2990 (2009)
© 2009 UICC

Systemic delivery of siRNA specific to tumor mediated by atelocollagen: Combined therapy using siRNA targeting Bcl-xL and cisplatin against prostate cancer

Ping Mu[1], Shunji Nagahara[2], Naoki Makita[2], Yuzo Tarumi[3], Kenji Kadomatsu[1] and Yoshifumi Takei[1,4]*

[1]*Department of Biochemistry, Nagoya University Graduate School of Medicine, Nagoya, Japan*
[2]*Formulation Laboratories Technology Research and Development Center, Dainippon Sumitomo Pharma, Ibaraki, Japan*
[3]*Koken Co., Ltd, Tokyo, Japan*
[4]*Division of Disease Models, Center for Neurological Diseases and Cancer, Nagoya University Graduate School of Medicine, Nagoya, Japan*

The largest obstacle to the effective use of short interfering RNA (siRNA) in an animal body is the ability to deliver it to the target tissue. Here we showed a systemic delivery method of siRNA specific to pregrown solid tumors *via* atelocollagen. Atelocollagen facilitated the selective uptake of siRNA into the tumors when an siRNA/atelocollagen complex was administered intravenously to mice. We chose a Bcl-xL protein as a model target to prove the therapeutic efficacy of the atelocollagen-mediated method. Bcl-xL acts as an anti-apoptotic factor, which is overexpressed in many cancers, including prostate cancer. One of the four designed siRNAs to human Bcl-xL potently inhibited the expression of Bcl-xL by the PC-3 human prostate cancer cell line *in vitro*, leading to cell apoptosis. Intravenous injections for 3 consecutive days (siRNA, 100 μg/injection per day as a complex with atelocollagen) effectively downregulated Bcl-xL expression in the PC-3 xenograft. We administered four series of 3 consecutive days of intravenous injections each, for a total of 12 injections, which significantly inhibited tumor growth when the treatment was combined with cisplatin (2 mg/kg). Local injection of Bcl-xL siRNA also potently inhibited tumor growth. All of the tumors treated with Bcl-xL siRNA/atelocollagen complex *via* both intravenous and intratumoral injection showed terminal deoxynucleotidyl transferase-mediated dUTP nick-end labeling-positive apoptosis. There were no severe side effects such as interferon-α induction and liver or renal damage in mice. Our results indicate that systemic delivery of siRNA *via* atelocollagen, which specifically targets tumors, is safe and feasible for cancer therapy.
© *2009 UICC*

Key words: short interfering RNA; Bcl-xL; apoptosis; drug delivery system; atelocollagen

RNA interference (RNAi) has revealed highly sequence-specific gene silencing in which short pieces of double-stranded RNA, *i.e.*, short interfering RNA (siRNA), suppress the expression of genes exhibiting sequence homology.[1,2] An intense research effort is under way to develop siRNAs as therapeutics for many kinds of diseases.[3] However, the largest obstacle to develop a therapy using siRNAs lies in the necessity of achieving effective delivery to the target organ and tissue. Thus, the major limitation for the use of siRNA *in vivo* is the inability of naked siRNA to passively diffuse through cellular membranes; *i.e.*, there is a strong anionic charge of the phosphate backbone and consequent electrostatic repulsion from the anionic cell membrane surface.[4] The other obstacles to the delivery of siRNAs *in vivo*, such as degradation by nuclease(s) in blood and interaction with blood components, indeed exist.[5] To overcome these obstacles, many delivery systems, such as hydrodynamic approaches[6] and bioconjugating approaches including cationic liposomes,[7] cationic polymers,[8] and cell penetrating peptides,[9] have been developed. However, thus far there is little conclusive method.

We and Ochiya's group previously showed the efficacy of atelocollagen for delivering nucleic acid compounds such as antisense oligodeoxynucleotides,[10–12] morpholino antisense oligomers,[13] and siRNAs,[14–16] especially *in vivo*. Atelocollagen, which is prepared from bovine dermis,[17,18] contributes to increases in cellular uptake, nuclease resistance and the prolonged release of siRNA,[14,19–21] as well as plasmid DNA,[17] and antisense oligonucleotide compounds,[10,11,13,22] administered to tumors. An siRNA–atelocollagen complex also can be delivered *via* an intravenous injection route as nanoparticles, enabling systemic delivery of siRNAs.[23] Takeshita *et al.*[23] previously showed the evidence of tumor targeted delivery of systemically administered siRNA with atelocollagen using functional image analysis. They used siRNA to luciferase and luciferase-expressing bone-metastatic tumor models *via* intracardiac injection.[23] More recently, we also successfully showed a therapeutic effect on inflammatory disease *via* atelocollagen-mediated systemic administration of siRNA targeting monocyte chemoattractant protein-1 (MCP-1).[16] However, little information is available about treating pregrown xenografted solid tumors by this modality, *i.e.*, adequate dose, frequency and interval of siRNA injections, although there is a lot of information about local injection to treat tumors.

In this study, we determine a modality to treat a pregrown xenograft derived from human prostate cancer cell line PC-3, *via* atelocollagen-mediated systemic administration in comparison with local administration. We chose Bcl-xL as a target. Bcl-xL, a major member of the Bcl-2 family, is well characterized as an anti-apoptotic protein. Overexpression of the Bcl-xL protein is observed in many cancers,[24] including prostate cancer,[25,26] leading to their desensitization to chemotherapy.[27–30] Thus, we determined a functional siRNA targeting human Bcl-xL to downregulate its expression in PC-3 cells, and a modality for the delivery of siRNA to treat PC-3 xenografts in nude mice *in vivo via* atelocollagen-mediated systemic administration without any severe side-effects. Finally, we showed the therapeutic effect of the siRNA on the xenografts by the systemic method established in this study, by combining the siRNA treatment with cisplatin (CDDP). We also quantified the siRNA systemically delivered to the tumors and several normal organs; the amount in tumors was quite high compared with that in normal organs.

Abbreviations: siRNA, short interfering RNA; CDDP, cisplatin; IFN-α, interferon-α; TUNEL, terminal deoxynucleotidyl transferase-mediated dUTP nick-end labeling; RNAi, RNA interference; STS, staurosporine; HPRT1, hypoxanthine guanine phosphoribosyl transferase 1; ELISA, enzyme-linked immunosorbent assay; DAPI, 4′, 6-diamidino-2-phenylindole; FSP-1, fibroblast specific protein-1; pDCs, plasmacytoid dendritic cells; PE, phycoerythrin; FITC, fluorescein isothiocyanate; APC, allophycocyanine; poly(I:C), polyinosine-polycytidylic acid; AST, aspartate aminotransferase; ALT, alanine aminotransferase; BUN, blood urea nitrogen; PTX, paclitaxel.

Grant sponsor: Ministry of Education, Science, Sports, Culture, and Technology of Japan (21st Century COE grant); Grant number: 17016030; Grant sponsor: Japan Society for the Promotion of Science; Grant numbers: 17790185, 19590273.

***Correspondence to:** 65 Tsurumai-cho, Showa-ku, Nagoya 466-8550, Japan. Fax: +81-52-744-2065. E-mail: takei@med.nagoya-u.ac.jp

Received 8 September 2008; Accepted after revision 6 February 2009
DOI 10.1002/ijc.24382
Published online 23 February 2009 in Wiley InterScience (www.interscience.wiley.com).

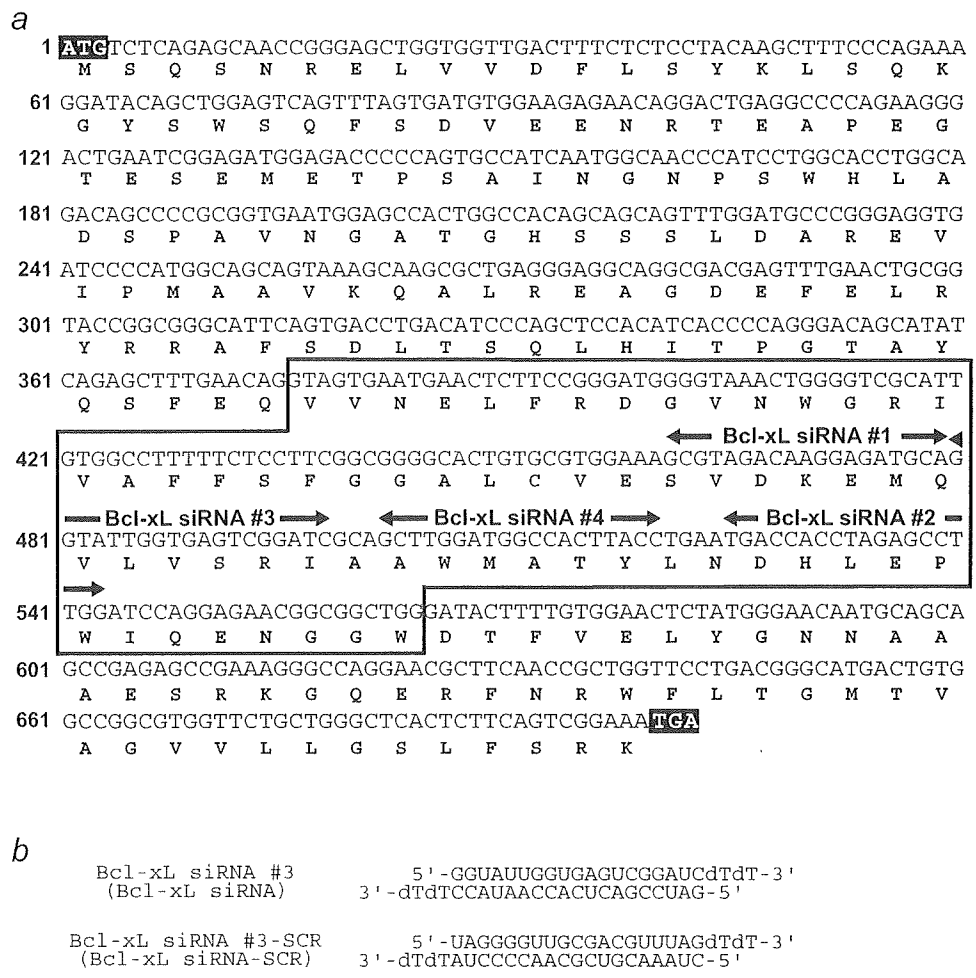

FIGURE 1 – (*a*) Design of the four siRNAs for human Bcl-xL. The locations of Bcl-xL siRNA #1, #2, #3 and #4 examined in this study are indicated by horizontal arrows. ATG (black box), the translation initiation site; TGA (black box), the translation terminal site; a black frame, the Bcl-xL-only region. (*b*) Structures of Bcl-xL siRNA #3, determined to be the most functional siRNA to downregulate human Bcl-xL in this study, and its scrambled control (Bcl-xL siRNA-SCR).

Material and methods

Cell culture and reagents

A human prostate cancer cell line, PC-3 (American Type Culture Collection, Manassas, VA), which shows an androgen-independent characteristic, was cultured in Ham's F-12 medium modified by Kaighn (F-12K) with 10% heat-inactivated fetal bovine serum at 37°C in a humidified atmosphere of 5% CO_2 as reported previously.[14,15] CDDP was obtained from Nippon Kayaku (Tokyo, Japan). Z-VAD-FMK and staurosporine (STS) were purchased from Sigma-Aldrich (St. Louis, MO).

siRNAs

Four siRNAs targeting human Bcl-xL mRNA (accession no. NM_138578) and one scrambled siRNA were designed. The sequences and locations are shown in Figure 1*a*. The siRNAs targeting Bcl-xL were designed using the sequences that were specific to Bcl-xL. We also used Bcl-xL siRNA-Cy3 to monitor the delivery efficiency and uptake in the PC-3 xenografts upon systemic injection. All siRNAs were synthesized by Dharmacon (Lafayette, CO).

Atelocollagen and siRNA/atelocollagen complex preparation

Atelocollagen is prepared from calf dermal collagen (Koken, Tokyo, Japan). Atelocollagen exhibits a stick-like structure, 300 nm in length, 1.5 nm in diameter and 300 kDa in molecular weight.[17] Atelocollagen shows neither antigenicity nor toxicity because it is free from antigenic telopeptides with pepsin treatment.[17] Atelocollagen is a liquid at 4°C and a gel at 37°C, when it is at a high concentration (≥0.5%). This biochemical feature of atelocollagen contributes to controlled release of siRNA directly injected into the tumor.[14,15,20] When atelocollagen is at a low concentration (0.05–0.1%), a coefficient of viscosity of atelocollagen (2.7 ± 0.2 mPa·S, $n = 3$; when a shear rate is 230 per sec) determined by E type viscometer becomes similar to that of blood. Thus, we used 0.5 and 0.05% of atelocollagen for local and systemic delivery of siRNA, respectively. The complex with siRNA forms a nano-sized particle (100–300 nm).[19] In the previous report, we showed the similar therapeutic efficacy of the VEGF siRNA/atelocollagen complex in different final concentrations (ranging 0.5–1.75%) of atelocollagen (Ref. 14 and unpublished results). For preparing the siRNA/atelocollagen complex, equal volumes of atelocollagen in PBS and siRNA solution were mixed by rotating for 20 min at 4°C.[14,16]

siRNA transfection in vitro

The siRNA transfection experiments mediated with Lipofectamine-Plus (Invitrogen, Carlsbad, CA) were performed as described previously.[14,15]

The siRNA transfection experiments mediated with atelocollagen were performed as reported previously.[19,23] Thus, an equal volume of siRNA solution (0.4 μM) and atelocollagen (160 μg/ml) was mixed for 20 min at 4°C. The final concentration of atelocollagen was 80 μg/ml. The siRNA/atelocollagen complexes were then pre-coated on 6-well plates (siRNA 100 pmol/0.5 ml per well). PC-3 cells were plated onto the siRNA/atelocollagen-complexes precoated 6-well plates at a density of 1×10^5 cells per well. Cell lysates were prepared 72 hr later.

RNA extraction, RT-PCR and real-time PCR

Total RNA was extracted from cells or from tumor tissues and was analyzed by RT-PCR and real-time PCR (qPCR) as described previously.[14,16] RT-PCR primers for human Bcl-xL, Bcl-2, Mcl-1 and Bax were designed according to the methods of Zhang *et al.*[31] and Komuro *et al.*,[32] respectively. The human Bcl-xS primers were 5′-GCTTTGAACAGGATACTTTTGTGG-3′ (forward) and 5′-AAGGCAATCTAGTCTCCTTTCTGG-3′ (reverse), under the following PCR conditions: 94°C for 30 sec, 55°C for 30 sec, 72°C for 1 min, 30 cycles. Real-time PCR primer and TaqMan probe for human Bcl-xL were designed according to the method of Ohga *et al.*[33] Results for Bcl-xL expression in real-time PCR analysis were normalized to hypoxanthine guanine phosphoribosyl transferase 1 (HPRT1, Applied Biosystems, Warrington, UK).

Western blot analysis

Cells were lysed with Buffer E (PBS with 1% NP-40, 0.5% sodium deoxycholate, 0.1% sodium dodecyl sulfate and 50 mM sodium fluoride) with a protease inhibitor cocktail (Sigma-Aldrich). The protein concentrations in lysates were determined with the Bio-Rad DC Protein Assay (Bio-Rad Laboratories, Hercules, CA). Equal amounts of lysate (30 μg/lane) were separated by 12% SDS-PAGE gels and transferred electrophoretically onto nitrocellulose membranes. The membranes were blocked with PBS containing 5% nonfat milk and 0.1% Tween 20 for 1 hr at room temperature and then incubated with mouse anti-human Bcl-xL antibody (BD Biosciences, Franklin Lakes, NJ) for 1 hr at room temperature. Finally, after the membranes were washed with PBS containing 0.1% Tween 20, they were incubated with horseradish peroxidase-conjugated goat anti-mouse IgG (Jackson ImmunoResearch Laboratories, West Grove, PA) for 1 hr. After further washing with PBS containing 0.1% Tween 20, the peroxidase activity was detected with an enhanced chemiluminescence detection system (Amersham Biosciences, Foster City, CA) according to the manufacturer's protocol.

Cell proliferation analysis

To determine the effect of Bcl-xL siRNA on cell proliferation, cells transfected with Bcl-xL siRNA or Bcl-xL siRNA-SCR were seeded in 96-well plates at a density of 1×10^4 cells per well. Twelve hours later, the medium was changed to serum-free medium. At the indicated time points, cell viability was determined with a cell counting kit (Dojin, Kumamoto, Japan). To determine the effect of Bcl-xL siRNA in combination with CDDP, the cells were incubated with CDDP (12 μM) at 48 hr post-transfection. At the indicated time points, cell viability was determined.

Caspase-3 activity assay

The PC-3 cells were incubated with or without Z-VAD-FMK (50 μM) after transfection with Bcl-xL siRNA or Bcl-xL siRNA-SCR. At 72 hr post-transfection, caspase-3 activity was determined using the CPP32/Caspase-3 Colorimetric Protease Assay Kit (MBL, Nagoya, Japan). Briefly, the cells were washed with cold PBS and then were suspended in chilled cell lysis buffer. After incubation on ice for 10 min, the cell lysate was centrifuged for 1 min at 10,000*g*. The supernatant was transferred to a fresh tube and was diluted into a protein concentration of 2 mg/ml in 50 μl cell lysis buffer. Then 50 μl of 2 × reaction buffer and 5 μl of the 4 mM DEVD-pNA substrate were added to each sample, followed by incubation at 37°C for 2 hr. The absorbance of each sample at 405 nm was measured.

Bcl-xL ELISA

The tumor tissues were homogenized in CelLytic-MT Mammalian Tissue Lysis/Extraction Reagent (Sigma) with a protease inhibitor cocktail. The cell lysate was centrifuged and the supernatant was harvested. The total protein concentrations in the cell lysates were determined with the Bio-Rad DC Protein Assay. The Bcl-xL protein levels in the tumors were determined using a Human Total Bcl-xL DuoSet IC ELISA Kit (R&D Systems, Minneapolis, MN) according to the manufacturer's instructions. The protein concentration of Bcl-xL was normalized to total protein concentration.

Terminal deoxynucleotidyl transferase-mediated dUTP nick-end labeling assay

After transfection with Bcl-xL siRNA or Bcl-xL siRNA-SCR 48 hr later, the cells were re-seeded into 8-chamber plates at a density of 3×10^4 cells per chamber and treated with CDDP (12 μM) either alone or in the presence of Z-VAD-FMK (50 μM). Another 72 hr later, terminal deoxynucleotidyl transferase-mediated dUTP nick-end labeling (TUNEL) assay was performed according to the manufacturer's protocol (MBL, Nagoya, Japan). For tumor tissue samples, sections (4 μm) were cut with a cryostat and then fixed in acetone. A TUNEL assay for tissue sections was performed as described previously.[15] Total cell numbers were determined by staining with 4′, 6-diamidino-2-phenylindole (DAPI). Images of the sections (green, TUNEL-positive cells; blue, nuclear fluorescence) were collected by fluorescence microscopy (Olympus, Japan) and TUNEL-positive cells were counted with MetaMorph software (Universal Imaging, Downing town, PA).

Xenograft models in nude mice

PC-3 cells (3×10^6) in 0.3 ml of serum-free F-12K medium were subcutaneously inoculated into the right flank of 8-week-old athymic nude mice (SLC, Tokyo, Japan).[13–15,34] After 3 weeks, when the tumors reached a volume of approximately 50–80 mm^3, the mice were divided randomly into multiple treatment groups.

In the experiments with local administration of Bcl-xL siRNA, the final concentration of atelocollagen was 0.5%. The intratumoral (it) injection of a naked siRNA (1 nmol, 13.3 μg) or siRNA (1 nmol, 13.3 μg) mixed with atelocollagen was administered once per week for 4 weeks. CDDP (2 mg/kg) was administered *via* intraperitoneal (ip) injection 2 days after the siRNA injection. The final volume of the Bcl-xL siRNA/atelocollagen complex for intratumoral injection was always 50 μl. Thus, the final concentration of Bcl-xL siRNA/atelocollagen was 13.3 μg/50 μl per tumor in 0.5% atelocollagen.

In the experiments with the systemic administration of Bcl-xL siRNA, the final concentration of atelocollagen was 0.05%. The intravenous (iv) injection of a naked siRNA (100 μg) or siRNA (100 μg) mixed with atelocollagen was administered on 3 consecutive days per week for 4 consecutive weeks. CDDP was administered *via* ip injection 1 day after the last injection of siRNA in each administration week. The final volume of the Bcl-xL siRNA/atelocollagen complex for intravenous injection was always 200 μl. Thus, the final concentration of Bcl-xL siRNA/atelocollagen was 100 μg/200 μl per mouse in 0.05% atelocollagen.

At regular intervals, tumor diameters were measured with digital calipers and the tumor volume was calculated with the formula: volume = $(\text{width})^2 \times \text{length}/2$.[14] All animals were managed according to the guidelines of the Institute for Laboratory Animal Research, Nagoya University Graduate School of Medicine.

Quantification of Bcl-xL siRNA in PC-3 xenograft as well as several organs after intravenous injection

To monitor the distribution of Bcl-xL siRNA in tumors, nude mice bearing PC-3 xenografts (tumor volume = 50–80 mm^3) were intravenously injected with 100 μg of Bcl-xL siRNA/atelocollagen complex. Fifteen, 30, or 60 min later, the mice were allowed to bleed, and then PC-3 xenografts and several organs (liver, kidney, lung, spleen and brain) were excised. Each sample was homogenized in Gentra Puregene Cell Lysis Solution (Qiagen, Hilden, Germany), and lysate was purified by Gentra Puregene Protein Precipitation Solution (Qiagen). Fluorescence labeled oligoribonucleotide (5′-GGUAUUGGUGAGUCGGAUC-3′) specific for the antisense strand of the Bcl-xL siRNA was added to the deproteinized lysates, and was allowed to form

hybrid. Amount of siRNA in the lysates was estimated for amount of hybrid quantitated by reverse-phase HPLC.

Analyses of tumor administered Cy3-labeled Bcl-xL siRNA

Nude mice bearing PC-3 xenografts were intravenously injected with a Cy3-labeled Bcl-xL siRNA (100 μg) with or without atelocollagen. Twenty-four hours later, tumors were excised and then sections (4 μm) were cut with a cryostat and then fixed in acetone. Nuclei, endothelial cells, and fibroblasts were stained with DAPI, anti-mouse CD31 rat monoclonal antibody (BD Pharmingen, San Diego, CA) and anti-mouse S100A4/FSP-1 antibody (Lab Vision/Neomarker, Fremont, CA), respectively. All positive signals were visualized with an fluorescein isothiocyanate (FITC)-labeled goat anti-rat IgG (Cappel Laboratories, West Chester, PA), or Alexa488-labeled goat anti-rabbit IgG (Invitrogen).

Measurement of interferon-α induction in plasmacytoid dendritic cells or in nude mice

For *in vitro* interferon (IFN)-α induction experiments, plasmacytoid dendritic cells (pDCs) were prepared from mouse spleens with a Plasmacytoid DC Isolation Kit II (Miltenyi Biotec, Bergisch Gladbach, Germany) according to the previous reports.[35,36] Thus, the cells collected from spleen were blocked with an FcR Blocking Reagent, and then incubated with Plasmacytoid Dendritic Cell Biotin Cocktail. After washing, the cells were mixed with Anti-Biotin Microbeads followed by magnetic separation with an LS column. Purified pDCs (mPDCA-1$^+$, B220$^+$ and CD11c^{low}) were determined by FACS with anti-mPDCA-1-PE, anti-CD11c-FITC and anti-CD45R (B220)-APC antibodies (Miltenyi Biotec). The purity was around 90%. pDCs were seeded into a 96-well plate at a density of 1×10^5 per well in RPMI-1640 (Invitrogen) with 10% FBS. pDCs were treated with 50 μg/ml of Bcl-xL siRNA with or without atelocollagen (0.05%). As a positive control, 50 μg/ml of polyinosine-polycytidylic acid (poly(I:C), Invivo Gen, San Diego, CA) was added. Each medium was collected after 24 hr of the addition.[36]

For *in vivo* IFN-α induction experiments, nude mice were intravenously injected with 100 μg of Bcl-xL siRNA with or without atelocollagen. As a positive control, 100 μg of poly(I:C) alone was injected. Blood was harvested 6 hr post-injection.

The mouse IFN-α concentration in the medium and serum was determined with a mouse IFN-α ELISA kit (PBL Biomedical Laboratories, Piscataway, NJ).

Measurement of liver enzyme and renal function in nude mice

For acute liver and renal function experiments, nude mice were intravenously injected with 100 μg of Bcl-xL siRNA/atelocollagen complex only or in combination with CDDP (2 mg/kg). As a positive control of acute liver damage, 0.4 g/kg of carbon tetrachloride (CCl_4, Wako Pure Chemical Industries, Osaka, Japan) dissolved in olive oil (1:10, v/v) was injected ip, and blood was taken 24 hr later.[37]

Liver and renal function was also evaluated 7 days later after siRNA injection. Nude mice were intravenously injected with 100 μg of Bcl-xL siRNA/atelocollagen complex only on 3 consecutive days (days 0–2) or in combination with CDDP (2 mg/kg, day 3) and blood was taken on day 7.

The levels of aspartate aminotransferase (AST), alanine aminotransferase (ALT), blood urea nitrogen (BUN) and creatinine in serum were measured by SRL Aichi Laboratory (Japan).

Statistical analysis

Statistical significance was determined using the Student's *t*-test. $p < 0.05$ was considered statistically significant.

Results

Bcl-xL siRNA specifically suppressed the expression of Bcl-xL in PC-3 cells

We first selected an effective siRNA by transfecting four Bcl-xL siRNAs into PC-3 cells. Bcl-xL siRNA #3 showed more than 99% knockdown efficiency in Bcl-xL protein expression after transfection with LipofectAMINE-Plus into PC-3 cells (Fig. 2*a*). We thus selected Bcl-xL siRNA #3 (termed Bcl-xL siRNA, Fig. 1*b*) as the most functional one and used it in future study. Bcl-xL siRNA almost eliminated both the expression of Bcl-xL in protein and its mRNA level, whereas scramble siRNA (Bcl-xL siRNA #3-SCR) did not decrease either the protein expression or the mRNA level (Figs. 2*b*,2c). Using RT-PCR, we determined whether or not Bcl-xL siRNA had any influence on the expression levels of other Bcl-2 family members. There were no changes in the expression of Bcl-xS, Bcl-2, Mcl-1, or Bax (Fig. 2*c*). The transfection of Bcl-xL siRNA *via* atelocollagen also successfully inhibited the expression of Bcl-xL like LipofectAMINE-Plus (Fig. 2*d*). The results revealed that Bcl-xL siRNA had a specific inhibitory effect on the expression of Bcl-xL, but no effect on other Bcl-2 family members examined in this experiment.

Downregulation of Bcl-xL reduced cell growth and enhanced chemosensitivity to CDDP in PC-3 cells

We transfected Bcl-xL siRNA or Bcl-xL siRNA-SCR into PC-3 cells, and determined cell growth 48 hr after transfection. Comparing the cell growth curve of the cells transfected with Bcl-xL siRNA against that of the cells transfected with Bcl-xL siRNA-SCR, we found that Bcl-xL siRNA significantly inhibited cell growth ($p < 0.001$; Fig. 3*a*).

Before the combinational experiments with CDDP *in vitro*, we treated PC-3 cells with various concentrations (0, 0.2, 0.8, 3.2, 12 or 50 μM) of CDDP. The cells treated with 50 μM of CDDP showed a strong reduction (78 %) in cell viability compared with no treatment group. On the other hand, the cells incubated with 12 μM of CDDP showed a weak reduction (23 %). Thus, we determined the concentration of CDDP (12 μM) to combine with Bcl-xL siRNA. As shown in Figure 3*a*, Bcl-xL siRNA showed significantly decreased cell viability in a time-dependent manner when combined with CDDP ($p < 0.001$). On the other hand, Bcl-xL siRNA-SCR showed no such effects.

Bcl-xL siRNA increased apoptosis in PC-3 cells in vitro

To investigate whether or not the anti-proliferative effect of Bcl-xL siRNA was accompanied by the induction of apoptosis, we performed TUNEL staining in PC-3 cells. As shown in Figure 3*b*, the proportion of TUNEL-positive cells was significantly higher in the PC-3 cells treated with Bcl-xL siRNA ($p < 0.001$) than in those treated with Bcl-xL siRNA-SCR. In the cells cotreated with Z-VAD-FMK, a broad caspase inhibitor, TUNEL-positive cells were significantly reduced ($p < 0.001$). Similar results were obtained when the siRNA treatment was combined with CDDP (Fig. 3*b*). We proved that downregulation of Bcl-xL induced caspase-3-dependent apoptosis in PC-3 cells (Fig. 3*c*).

Determination of a suitable dose of CDDP for in vivo *therapeutic experiments*

To determine the therapeutic effectiveness of Bcl-xL siRNA/CDDP *in vivo*, we first analyzed the effect of the treatment with CDDP alone. Two doses of CDDP (2 or 4 mg/kg) were intraperitoneally injected into mice once a week. The tumor volumes were measured twice per week. The group treated with 2 mg/kg of CDDP showed a moderate inhibition of tumor growth, whereas the group treated with 4 mg/kg of CDDP showed potent inhibition compared with the untreated group (Fig. 7).

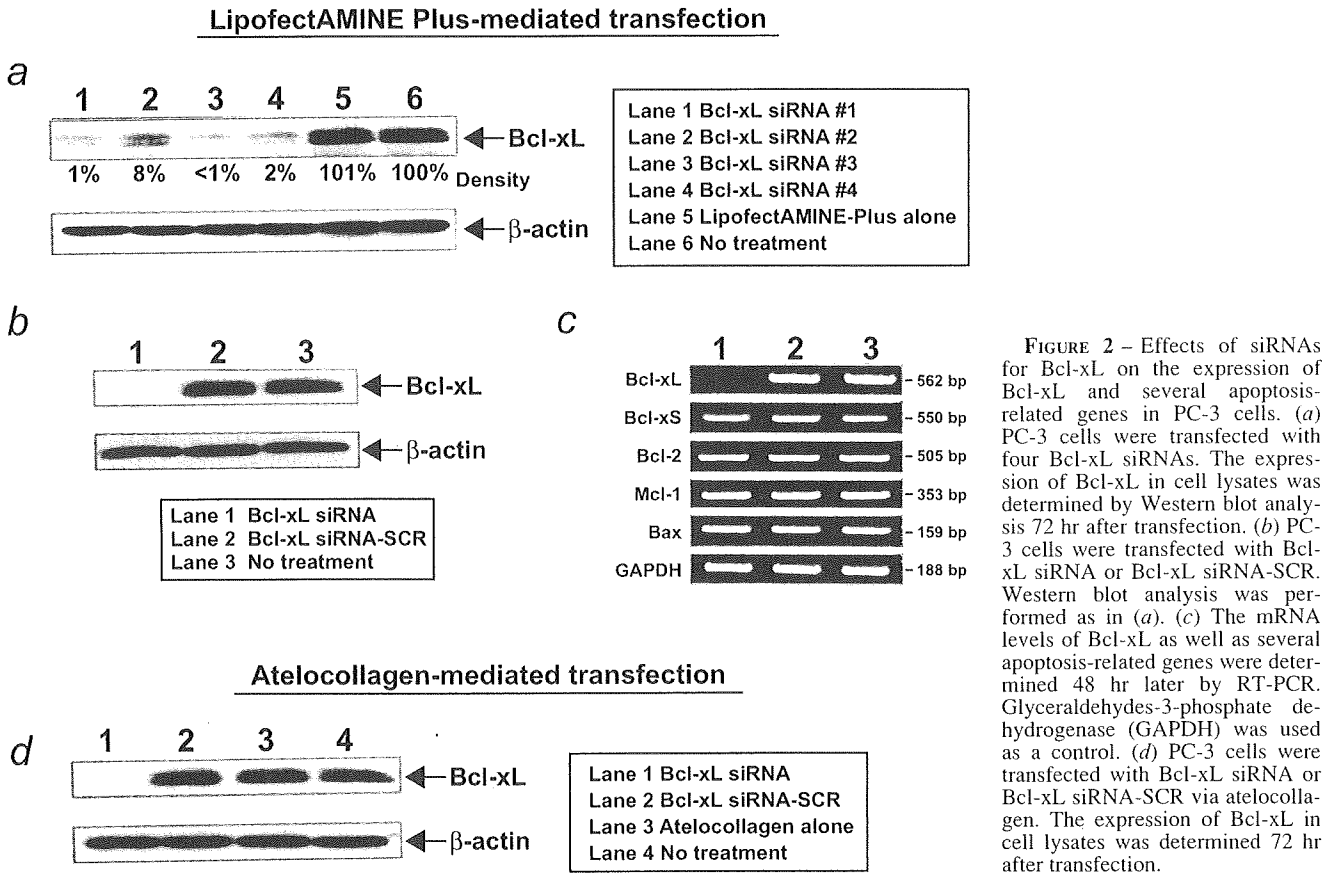

FIGURE 2 – Effects of siRNAs for Bcl-xL on the expression of Bcl-xL and several apoptosis-related genes in PC-3 cells. (*a*) PC-3 cells were transfected with four Bcl-xL siRNAs. The expression of Bcl-xL in cell lysates was determined by Western blot analysis 72 hr after transfection. (*b*) PC-3 cells were transfected with Bcl-xL siRNA or Bcl-xL siRNA-SCR. Western blot analysis was performed as in (*a*). (*c*) The mRNA levels of Bcl-xL as well as several apoptosis-related genes were determined 48 hr later by RT-PCR. Glyceraldehydes-3-phosphate dehydrogenase (GAPDH) was used as a control. (*d*) PC-3 cells were transfected with Bcl-xL siRNA or Bcl-xL siRNA-SCR via atelocollagen. The expression of Bcl-xL in cell lysates was determined 72 hr after transfection.

Local or systemic administration of Bcl-xL siRNA via *atelocollagen effectively suppressed the expression of Bcl-xL* in vivo

To evaluate the effects of Bcl-xL siRNA, intratumoral treatment and intravenous treatment with Bcl-xL siRNA, together in either case with atelocollagen, were performed. Bcl-xL siRNA was injected, it or iv, into mice bearing PC-3 xenografts (tumor volume = 50–80 mm^3). The kinetics of downregulation of Bcl-xL expression is demonstrated with real-time PCR and ELISA. Real-time PCR showed that the expression levels of Bcl-xL in the tumors decreased to 12 and 21% after intratumoral injection with 1 nmol (13.3 μg/tumor) and 0.5 nmol (6.7 μg/tumor) of Bcl-xL siRNA with atelocollagen, respectively, and the results were confirmed by ELISA (Fig. 4*a*).

For systemic administration of Bcl-xL siRNA, we injected 100 μg of Bcl-xL siRNA into the tail vein one time, consecutively two times and consecutively three times, respectively (Fig. 4*b*). The real-time PCR showed that the three consecutive injections of the siRNA with atelocollagen suppressed expression of Bcl-xL to 49%, which was better than one injection (65%) or two consecutive injections (55%; Fig. 4*b*). Similar results were obtained by ELISA. The different doses of Bcl-xL siRNA were also examined in this experiment (Fig. 4*c*). Three consecutive injections with 100 μg of Bcl-xL siRNA with atelocollagen significantly suppressed the expression of Bcl-xL compared with 50 μg ($p < 0.05$), and showed an inhibitory effect similar to 200 and 400 μg (Fig. 4*c*). On the basis of these results, we made therapy schedules for *in vivo* experiments with dose and injection intervals as shown in Figs. 5*a* and 6*a*.

Local administration of Bcl-xL siRNA showed a significant anticancer effect in PC-3 xenografts

Intratumoral injection of Bcl-xL siRNA with or without atelocollagen was repeated every 7 days (total four times). We combined Bcl-xL siRNA with 2 mg/kg of CDDP, which has shown a moderate anticancer effect (data not shown). As shown in Fig. 5*b*, Bcl-xL siRNA with atelocollagen inhibited tumor growth and significantly enhanced the anticancer effect of CDDP ($p < 0.001$) compared with Bcl-xL siRNA-SCR. At the end of the study (on day 28), all mice were killed and the tumors were weighed. The local administration of Bcl-xL siRNA/atelocollagen led to a remarkable inhibition of tumor weight, whereas an injection of a naked Bcl-xL siRNA showed no significant effect on the tumor growth (Figs. 5*b*, 5*c*). No body weight loss was found during the experimental period (data not shown). TUNEL staining revealed the induction of apoptosis in xenografts treated with Bcl-xL siRNA/atelocollagen (Fig. 5*d*). Local administration of atelocollagen alone had no effect on the tumor growth, microvessel density and cell apoptosis of PC-3 xenograft consistent with our previous reports.[14,15]

Systemic administration of Bcl-xL siRNA showed a significant anticancer effect in PC-3 xenografts

The therapeutic effects of systemic administration of Bcl-xL siRNA with or without atelocollagen were also tested by intravenous injection of Bcl-xL siRNA into the tail veins of mice bearing PC-3 xenografts. Systemic administration of Bcl-xL siRNA/atelocollagen complex significantly suppressed tumor growth ($p < 0.001$), and showed a greater inhibitory effect when in combination with CDDP (Figs. 6*b*, 6*c*). On the other hand, systemic administration of a naked Bcl-xL siRNA showed no effect on tumor growth. As shown in Figure 6*d*, the xenografts treated with systemic administration of Bcl-xL siRNA with atelocollagen plus CDDP showed more TUNEL-positive cells compared with Bcl-xL siRNA-SCR with atelocollagen plus CDDP.